Electronic Properties of Single Wall Carbon Nanotubes with Introduction to Apertureless Near Field Scanning Optical Microscopy

Thesis by
Habibe Durmaz

In Partial Fulfillment of the Requirements
for the
Degree of Master of Arts

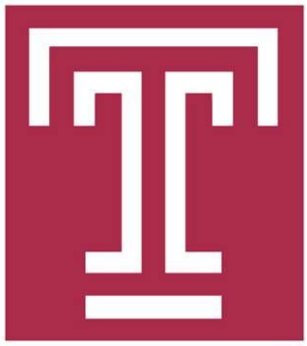

Department of Physics
College of Science and Technology
Temple University
Philadelphia, Pennsylvania
2010

(Submitted 20 June 2010)

Electronic Properties of Single Wall Carbon Nanotubes with Introduction to Apertureless Near Field Scanning Optical Microscopy

Thesis by
Habibe Durmaz

Department of Physics
College of Science and Technology
Temple University

In Partial Fulfillment of the Requirements
for the
Degree of Master of Arts

Dr. Eric Borguet (Advisor)
Professor in Department of Chemistry
Temple University

Dr. Theodore W. Burkhardt
Department of Physics
College of Science and Technology
Temple University

Dr. A. Marjatta Lyyra
Department of Physics
College of Science and Technology
Temple University

Acknowledgements

I consider myself extremely lucky to have counted with the help and support from many individuals throughout my graduate endeavor at Temple University. This thesis is the culmination of two years of work. This small portion of it is my opportunity to thank the friends and colleagues who helped me through these years. I learned a great deal from them and will always be very grateful.

First, I would like to thank my advisor Prof. Dr. Eric Borguet for entrusting me with this project. It has allowed me to bring together many of my seemingly disparate interests into a single piece of work, with a level of integration I would not previously have expected. The idea seemed simple enough at the time.

Also, I would like to thank Dr. Theodore W. Burkhardt, who brought me to Temple University, for his attentive mentoring and his guidance throughout the research portion of my graduate studies. He was always in the best disposition to offer advice and always put himself available for help, even when his schedule was not the most flexible.

I truly appreciate his support Dr. Peter Riseborough, Dr. Marjatta Lyyra, and Dr. Dimitri Romanov as well as the rest of the professors who taught the required academic courses for the master program. They very effectively helped me focus on academic weaknesses and helped develop my academic problem solving skills and critical thinking.

I would like to say thank you to one of my best friends, Sinan Sagir, who is physically far away from me, but always next to me. His assistance and valuable advice could not be overstated.

In the lab, I have had the chance to interact with and benefit from the help of many great minds. I am very grateful to lab-mate Nikolay Dementev answered questions in chemistry and Dr. Kim helped me to find and implement right solutions many times. Their new approaches to problem solving and analyzing were always very insightful. Their good humor and technical skills made working with them in the lab a very pleasant experience.

And last but not least, to all my friends and family, thank you as well. Your support was always there and it always made me feel a very lucky person. I hope you all know how much that meant to me!

Abstract

This thesis describes Scanning Tunneling Microscopy (STM) and Atomic Force Microscopy (AFM) experiments investigating the electronic density of state of HNO_3 treated, arc-discharged produced Single Walled Carbon Nanotubes (SWCNTs) in order to characterize them in ambient condition. STM continues to be a key method for characterizing SWCNTs, particularly in regards to their electronic properties.

The produced SWCNTs consist of bundles of metallic and semiconducting Single Walled Carbon Nanotubes (SWCNTs). The challenge in this work is to isolate individual tubes and determine the electronic density of states of SWCNTs in ambient conditions. Some studies show that the SWCNTs can be characterized by using Ultra High Vacuum STM (UHV-STM).

The primary aim of this work is to study SWCNTs and to familiarize with STM and AFM techniques. I also myself improved my skills of using Scanning Probe Microscopy (SPM) techniques to conduct Apertureless Near-Field Scanning Optical Microscopy (ANSOM) for my Ph.D and have included a review of this technique.

ÖZET

Bu tezde taramali tunelleme mikroskobu (STM) ve atomik kuvvet mikroskobunun (AFM) işlenmiş HNO_3 ve ark ateşleme metodu ile üretilmiş tek duvarlı karbon nanotüplerin (SWCNT) özellikleri çevre şartlarında açıklanmıştır. STM, SWCNT' leri karakterize etmede, özelliklede elektronik özelliklerin belirlenmesinde bir anahtar metod olmaya devam etmektedir.

Üretilen SWCNT'ler, metalik ve yarıiletken yapıdaki SWCNT' ler paketi şeklindedir. Bu çalışmadaki en büyük zorluk tek bir karbon tüpü karmaşık yapıdan ayırmak ve durum yoğunluğunu (DOS) çevre şartlarında belirleyebilmektir. Bazi calismalar, tek duvarlı karbon nanotüplerin özelliklerinin yüksek vakumlu STM (UHV-STM) kullanılarak belirlenebileceğini göstermektedir.

Bu çalışmanın temel amacı ise, tek duvarlı karbon nanotüpleri incelemek ve taramalı mikroskop çeşitleri olan STM ve AFM ile deneyim kazanmaktı. Aynı zamanda, bu çalışma ile doktora çalışmamda kullanacağım Açıklıksız Yakın-Alan Taramalı Optiksel Mikroskop (ANSOM) a bir ön çalışma olarak Taramalı Mil Mikroskobunu (SPM) kullanma becerilerimi geliştirdim ve bu tezde ANSOM tekniğinden genel olarak bahsettim.

TABLE OF CONTENTS

LIST OF FIGURES

CHAPTER 1

1. Introduction to SPM

Scanning probe microscopy (SPM) is unique among imaging techniques in that it provides three-dimensional real-space images. Subatomic resolution can be achieved under optimum conditions. A typical SPM consists of five parts: the tip, the scanner, the detector, the electronic control system, and a vibration isolation system. Beginning with scanning tunneling microscopy (STM), I will give brief introduction to SPM.

1.1. Introduction to Scanning Tunneling Microscopy (STM)

Scanning tunneling microscope (STM) is used for characterization of surface physical and chemical properties of conducting and semiconducting surfaces at atomic-scale resolution.

The essential elements of STM are a sharp metallic tip and a conducting sample over which the tip is scanned to create an image of the sample surface. The basis of scanning tunneling microscopy and spectroscopy is electron tunneling between the tip and the sample. Electron tunneling is a quantum mechanical phenomenon which is not found in classical physics. In a metal or semiconductor, electrons can exist within allowed energy ranges, shown by the shaded areas in Figure 1-a for the case of metals. In the space between two materials, there is an energy barrier, determined by

the material in the space. If a voltage difference is imposed between the two metals, the shape of energy barrier will be changed, as shown in Figure 1-b.

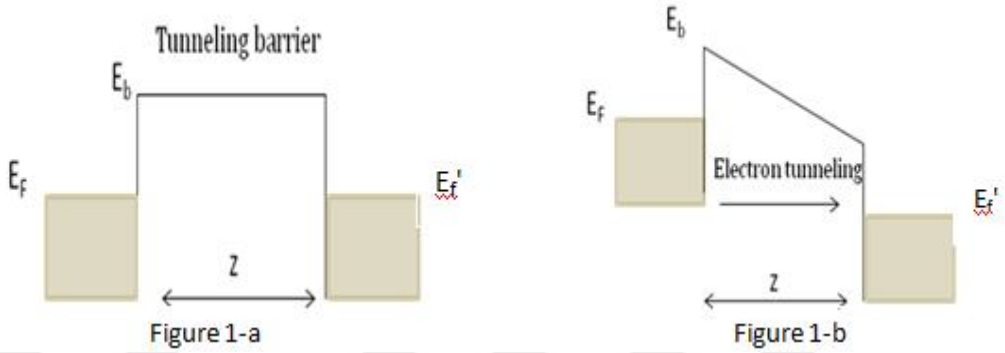

Figure 1.1 The energy levels in two metals separated by an insulating or vacuum barrier (a) with no bias applied between the solids and (b) with an applied bias. Shaded areas indicate the allowed energies of electrons, where is the Fermi energy, is the E_b shows energy barrier, the applied bias U is E_f-E_f', and z is the distance between the two solids.

Classically the electrons cannot travel across the barrier. However, quantum mechanics allows electron to traverse the barrier with a probability that decays exponentially with the thickness, z. To describe the system completely in quantum mechanics requires a wave function, which is a function of time and the coordinates of all the particles in the system and solves the Schrodinger equation.

The solutions to Schrödinger's equation inside the barrier have the form:

$$\psi(z) = \psi(0)e^{-kz} \tag{1}$$

where

$$k = \frac{\sqrt{2m(U-E)}}{\hbar} \tag{2}$$

and where m is the mass of an electron, ħ is Planck's constant divided by 2π, E is the energy of the electron, and U is the barrier potential. The probability per unit time that an electron will cross the barrier is the tunneling current I, which decays like the square of the wave function, i.e. Exponentially with the barrier width z as

$$I \sim e^{-2kz} \tag{3}$$

The exponentially decaying incident, and transmitted wave functions are shown in Figure 1.2.

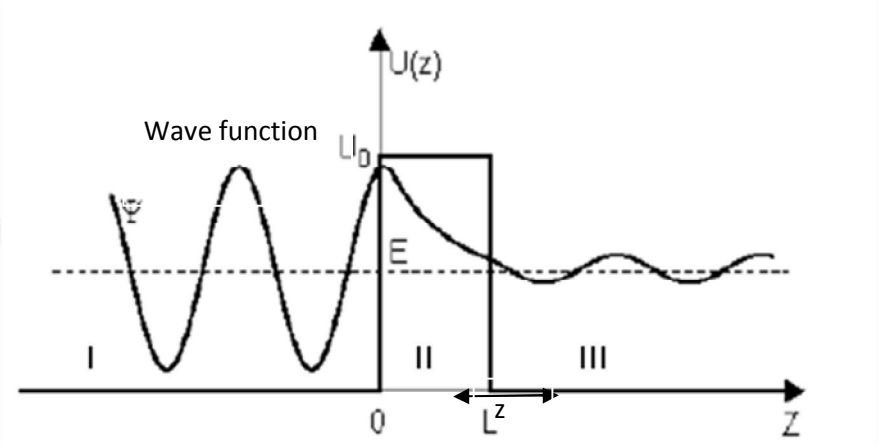

Figure 1.2 In region I incident and reflected, II transmitted, and III decaying wave functions are shown.[1]

When the STM tip and the sample are sufficiently close to each other, the wave functions overlap, and the resulting current is:

$$I \sim Ce^{-2kz} \tag{4}$$

where z is the tip-sample separation and C is a constant. The current depends exponentially on the tip-sample separation.

An STM image is obtained by scanning the tip over the surface of the sample without any ohmic contact between the tip and the sample since the tip is typically maintained at a height of 5 to 10 Å above the sample[2]. There are two operation modes, constant current and constant height. In constant current imaging, a feedback mechanism varies the tip-sample separation in order to maintain a constant current while a constant bias is applied between the tip and the sample. In the constant height mode, the tip vertical position is kept constant (effectively constant tip-sample separation), and a constant applied bias is applied while current is recorded. The images that are recorded indicate the height at a specific x, y position in the constant current mode and changes in the current as the tip scans the surface in the constant height mode.

STM Tunneling spectroscopy provides information about the electronic structure of the sample by probing the Density of States (DOS) as function energy, as discussed below.

1.2. Introduction to Atomic Force Microscopy (AFM)

Atomic force microscopy (AFM) is one of a family of scanning probe microscopes which has grown steadily since the invention of the scanning tunneling microscopy by

Binning and Rohrer in the early eighties, for which they received the Nobel Prize for Physics in 1986 [3, 4]

An atomic force microscope (AFM) is used to investigate sample properties at or near the sample surface. An AFM typically consists of a cantilever, a quadrant photo diode, a piezo-electric tube, and a diode laser. In the AFM technique, the sharp probe (tip) is scanned across a sample surface, in contact or in very close proximity to the surface, or the sample is scanned beneath the tip. The tip is usually a couple of tens of microns high and often less than 500Å in diameter, an example is shown in Figure 1.3.

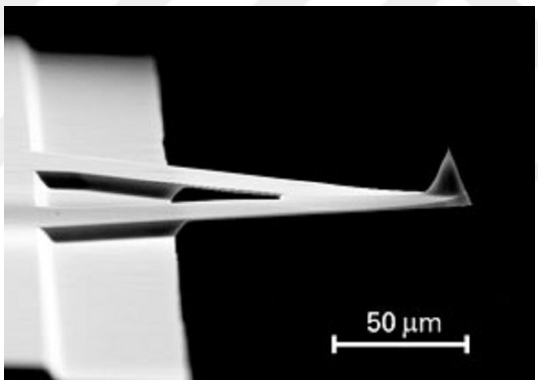

Figure 1.3 SEM image of triangular SPM cantilever with probe (tip). (Image from MikroMasch)[5]

During imaging, there are inter-atomic forces are active between the tip and the sample which cause the cantilever to bend or deflect.

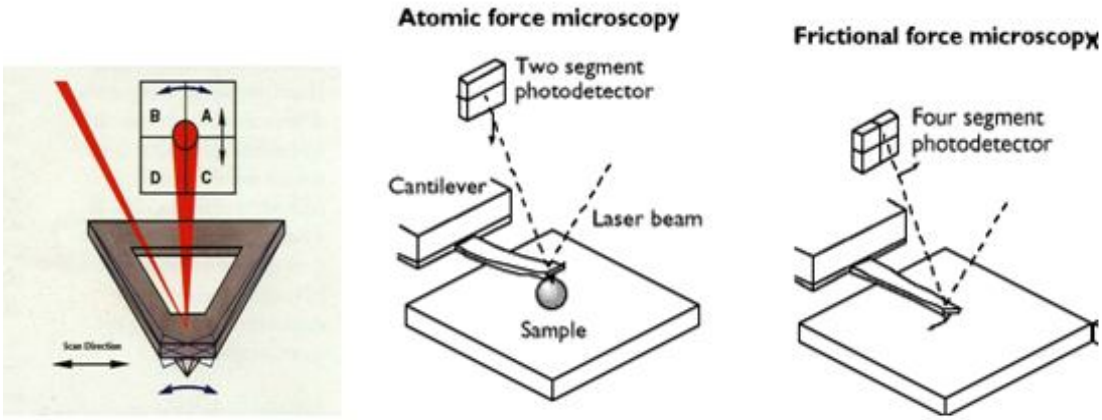

Figure 1.4 AFM internal laser is focused on the very end of back side of cantilever. Reflected laser beam from cantilever is detected by two and four (quadrant) segment photo diode[3].

The beam reflected from the top surface of the cantilever is positioned on a quadrant photodiode for beam deflection detection, as shown in Figure 1.4. From the differences of the photocurrents of the two (or four) segments of the quadrant diode, the deflection of the cantilever can be detected. This signal is called the "a - b" or "deflection" signal indicated in Figure 1.5. These deflections are recorded and processed using imaging software. The result is a topographical image of the sample. There are three different modes in AFM: contact (repulsive), tapping, and non-contact mode.

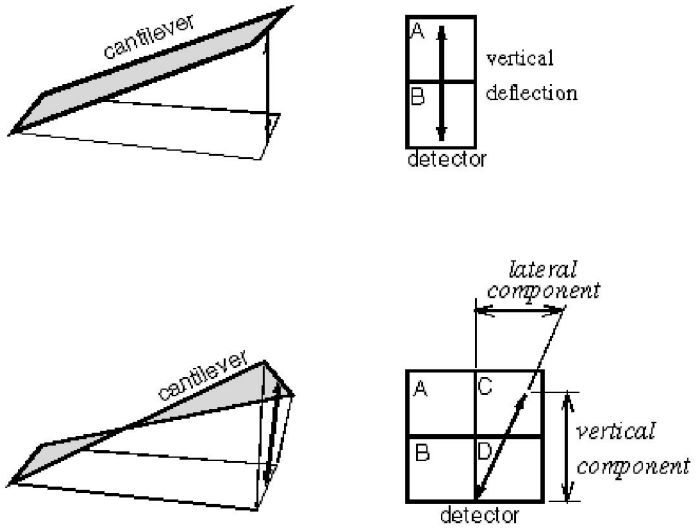

Figure 1.5 The lateral and vertical components of focused laser beam into AFM cantilever[3].

For using the quadrant photo diode is to determine both the lateral and vertical components of the tip deflection. As the light beam moves between the upper and lower pairs of segments, the deflection of the cantilever can be deduced from the treatment of all individual photocurrents using

$$\Delta I_{vertical} = (I_{upper\_left} + I_{upper\_right}) - (I_{lower\_left} + I_{lower\_right}) \quad (5)$$

I is the current from photo-quadrant. Usually the laser beam has a characteristic spot diameter which is proportional to the distance between the cantilever and the photodetector. The independence of the force sensor´s sensitivity of the separation of photodetector and cantilever allows the realization of very compact beam-deflection schemes.

1.2.1. Tapping Mode AFM

In the tapping mode, the probe assembly is driven so it oscillates at the resonance frequency of the cantilever by applying an AC voltage to the piezo-electric scanner. As the probe touches the sample, the amplitude and phase of the oscillation change in response to surface-related force gradients. By implementing the feedback loop shown in Figure 1.6, the tip oscillation amplitude can be maintained, and changes in oscillation phase can be eliminated.

An important function of the feedback electronics system is to generate a variable offset that depends on the probe's oscillation amplitude at driving frequency Ω. The signals V_{high} and V_{low} from the photodetector are used to generate an amplitude signal. This signal is used by the the proportional-integral correction circuit to generate a correction signal. This correction signal is fed back into the system through the probe holder of piezoelectric material. The piezoelectric material translates this signal into a change in the height of the AFM tip by deforming to restore the oscillation amplitude to the target value.

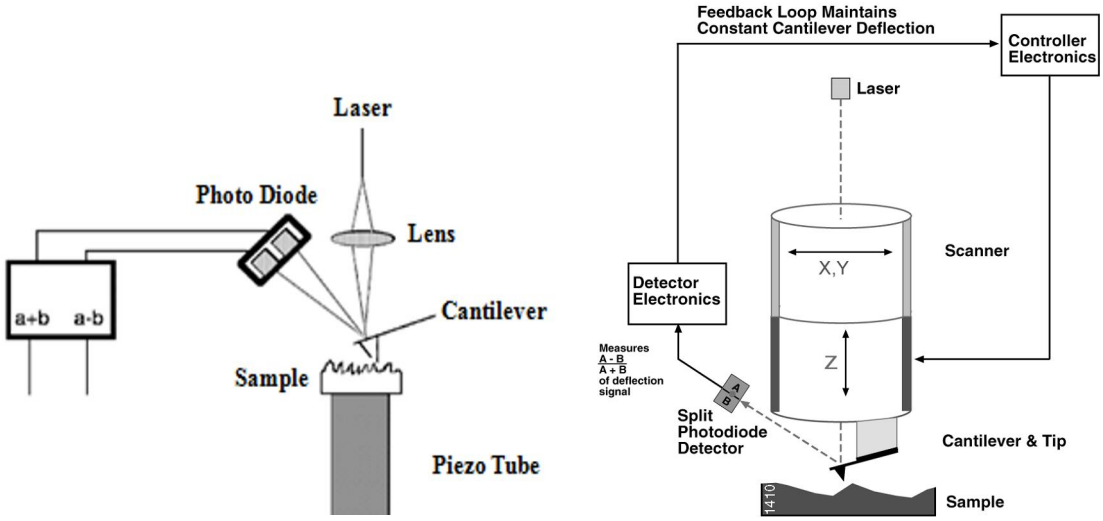

Figure 1.6 Important components of the atomic force microscope: A focused laser beam is reflected from the back of a cantilever to a position sensitive photo diode. a) The sample is mounted onto a piezo-ceramic tube and can be moved in x, y and z direction. b) Tip is raster scanned along sample.

1.2.2. Contact mode AFM

In this mode tip is attached to the end of cantilever, and the tip makes soft physical contact with the surface. The contact mode is also known as the repulsive mode. The tip is attached to the end of a cantilever with a low spring constant, smaller than the effective spring constant holding the atoms of the sample together. As the scanner traces the tip across the sample, the cantilever bends under the contact forces. From the cantilever deflection, image is generated.

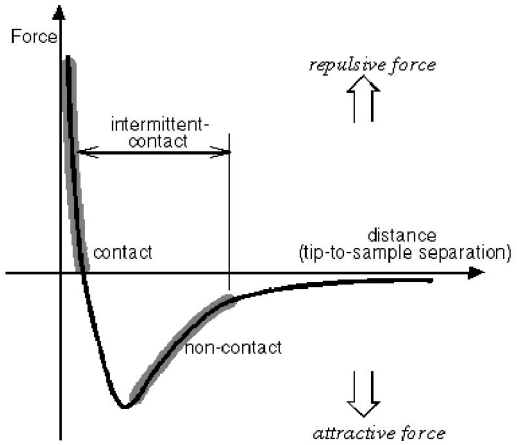

Figure 1.7 The parts of an approach-retraction cycle of the tip. In the contact regime, the cantilever is held less than a few Å from the sample surface, and the inter-atomic force between the cantilever and sample is attractive[3].

The force between the tip and the sample is represented in Figure 1.7. At the right side of the curve of Figure 1.7, the tip and the sample are separated by a large distance. As the tip approaches the sample, they first weakly attract each other. This attraction increases, but simultaneously their electron clouds begin to repel each other electrostatically, leading to a repulsive interaction at short distance.

1.3. Experiment with AFM

In many applications one would like to determine the chemical identity of individual molecules and examine the optical properties of material in nano scale with high resolution. In this thesis, I study the electronic density of states of Single Walled Carbon Nanotubes (SWCNTs) under ambient conditions and give an introduction to the technique of apertureless near-field scanning optical microscopy (ANSOM) that I plan to use in my Ph.D research. The density of states was determined by measuring

the electrical conductivity of the nanotubes, i.e., current versus voltage (I-V curve) dependence.

In this study, I worked with Atomic Force Microscopy (AFM) in the contact, tapping, and current sensing modes as well as STM (scanning tunneling current microscopy) in order to observe individual Single Walled Carbon Nanotubes (SWCNTs) with scanning tunneling spectroscopy (STS). After detecting individual CNTs either in AFM or STM, I-V curve was obtained. In AFM it is easy to image CNTs in the tapping mode, as shown in Figures 2.2 and 2.3. In the contact and current sensing AFM modes, this is not as easy, since CNTs are dragged by the tip while force is applied to the tip.

CHAPTER 2

2. Single Wall Carbon Nanotubes

2.1. What are Single Wall Carbon Nanotubes?

Carbon nanotubes can be considered as one single sheet of graphene rolled up along a given direction to form a tube (See Figure 2.1). Carbon nanotubes were first observed by Iijima (1991) while studying the surface of the carbon electrodes of an electric arc-discharge apparatus which had been used to make fullerenes C_{60}[6]. A nanotube exhibits extraordinary mechanical properties that make it ideal for reinforced composites. A CNT has a huge Young modulus, which makes it as stiff as diamond, and the estimated tensile strength is more than ten times that of steel wire with the same weight. Theoretical calculations first predicted that Single-Walled Carbon Nanotubes (SWNTs) could exhibit either metallic or semiconducting behavior depending only on diameter and helicity.[7, 8]

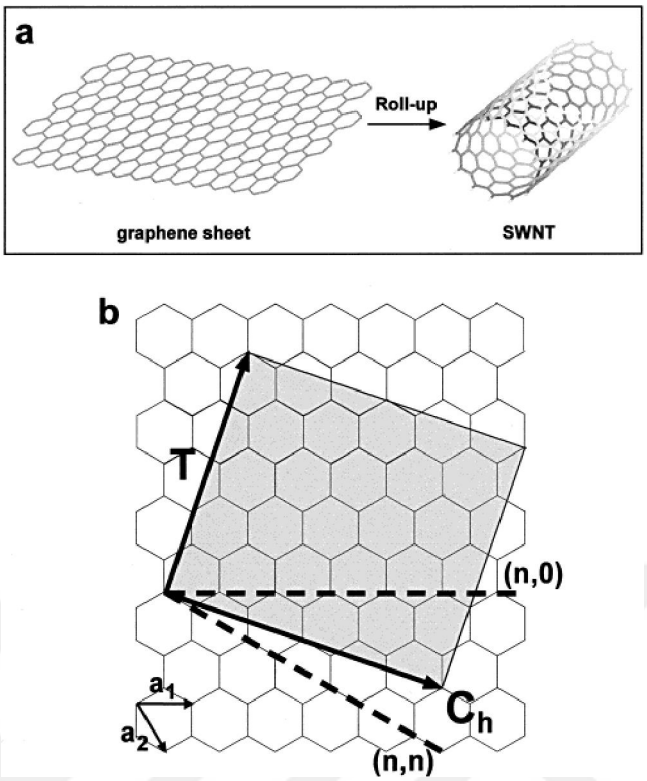

Figure 2.1 Schematic of a 2D graphene sheet illustrating lattice vectors a_1 and a_2, and the roll-up vector $Ch = na_1 + ma_2$. The limiting, achiral cases of (n,0) zigzag and (n,n) armchair are indicated with dashed lines. The translation vector T is along the nanotube axis and defines the 1D unit cell. The shaded, boxed area represents the unrolled unit cell formed (3) by T and Ch. The diagram is constructed for (n,m) (4,2).[7]

There are two ways to identify the physical properties of carbon nano tubes. One way is to look at the diameter and helicity of graphitic rings in their walls. The diameter and helicity of a SWNT are uniquely characterized by the roll-up vector $C_h = na_1 + ma_2 = (n,m)$, where a_1 and a_2 are the graphene lattice vectors and n and m are integers. The limiting, achiral cases, (n, 0) zigzag, and (n,n) armchair are indicated with dashed lines in Figure 1b. The translation vector T is along the tube axis and orthogonal to C_h, and its magnitude represents the length of the unit cell of an (n,m) tube. The rolled up area swept out by T and C_h (Figure 2.1-b, gray) corresponds to the repeat unit of an (n,m) tube. Thus, a nanotube's (n,m) symmetry

determines the size of its unit cell, which can vary greatly among tubes. Electronic band structure calculations can predict the (n, m) indices, which determine whether a SWCNT will be a metal or a semiconductor. SWCNTs are metallic if their indices satisfy the condition that (n-m)/3 is an integer; otherwise, the SWCNTs are semiconducting [9]. The other way is determining of their density of states (DOS). These states are formed as a result of delocalization of the 2s and 2p valence electrons of the carbon atom, so that 2s electrons in hybridization fill energy regions lying below and above the Fermi level, whereas 2p electrons fill a region near the Fermi level. As this takes place, a change in chirality and hence in the nanotube radius also causes a change in the energy gap.

High resolution STM images of SWCNTs reveal a graphite-like honey comb lattice that allows one to determine the n, m indices from the image. In the course of my experiments I wasn't able to get high resolution STM images of SWCNT. T.W. Odom and Kim obtained high resolution STM images of SWCNT in UHV STM in 1998[9]. Instead, I determined the I-V curve of each individual SWCNT by positioning the STM tip on the tubes. Scanning tunneling microscopy (STM) and spectroscopy (STS) can be used to locate and measure the band-gap of individual nanotubes.

2.2. Sample Preparation

Single Wall Carbon Nanotubes (SWCNT) were synthesized by using an arc-discharge method and purified with nitric acid. The average diameter of SWCNTs is around 1.4 nm and length is 1-2 microns. Carbon nanotubes always occur in bundles. To isolate the nanotubes, the bundles have to be disassembled by ultrasonication. Ethanol is a convenient solvent for SWCNTs since it evaporates quickly and there is no requirement for the sample to dry. Samples that are suitable for both STM and AFM studies were prepared by spin coating (5000 rpm) single wall carbon nanotube suspensions of ethanol onto HOPG (Highly Ordered Pyrolytic Graphite) and mica. Test samples (less than 1 mg) were dispersed in ethanol by using sonication for two hours and imaged by atomic force microscopy in contact, current, and tapping modes in order to see if they were individual tubes or bundles.

The SWCNT and ethanol solution were deposited on mica by using spin coating method at 5000 rpm, and the distribution of the tubes on the surface was studied with AFM as shown in Figure 2.2. The mica surface does not require complicated preparation since it naturally presents a flat featureless surface; it just needs to be cleaved by using scotch tape before deposition of the test sample.

2.3. Demonstration of AFM

Carbon nanotubes came in bundles consisting of metallic and semiconducting SWCNTs. The electronic properties of individual SWCNT can be determined by STS. However, in order to consider individual tubes one needs to investigate the height of nanotubes corresponding to ~ 1.4 nm for arc-produced nitric acid treated SWCNTs. Following the sample preparation explained above, we observed bundles of SWCNTs. After sixfold dispersion and dilution of the SWCNT, we were able to obtain individual SWCNTs, as shown Figure 2.4.

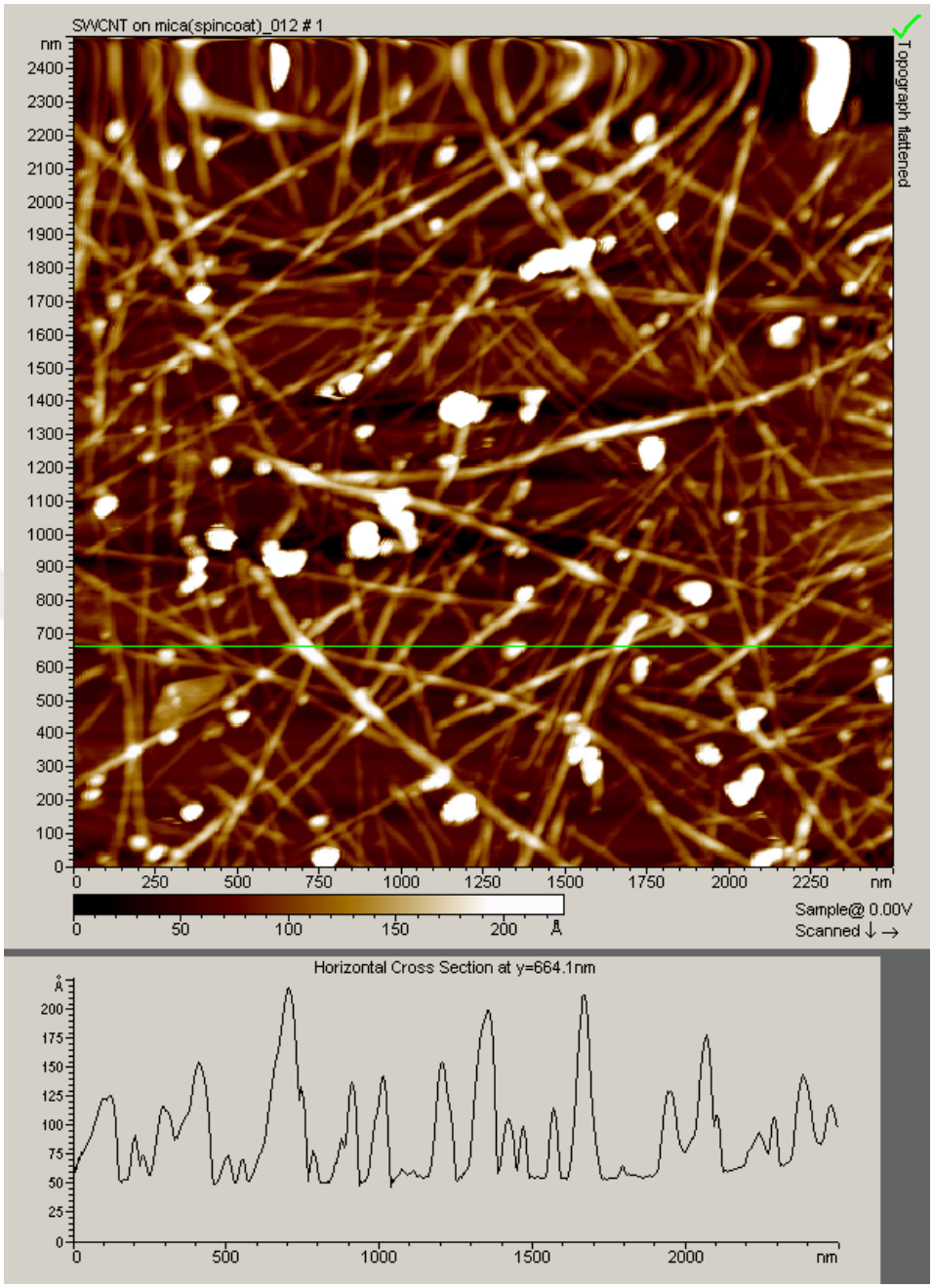

Figure 2.2 Image of single wall carbon nano-tubes deposited on mica, taken in AFM tapping mode. The SWCNTs are still bundled as can be seen by comparing the feature diameters (~10-15 nm high) with the individual SWCNT diameter, which is usually 1- 2 nm.

The topographical image (in Figure 2.2) shows that the SWCNTs are still bundled and therefore the test sample needs to be further dispersed in ethanol. According to

this AFM image of SWCNT shown in Figure 2.2 SWCNT solution is needed to be diluted with ethanol and dispersed by sonication. After dilution of the test sample five times with ethanol and dispersion with sonication for one hour for each dilution, the image shown in Figure 2.3 was obtained in AFM tapping mode. In contact mode AFM it is hard to image SWCNT since force applied tip causes to CNTs drag on the surface. For this reason the tapping mode is preferable.

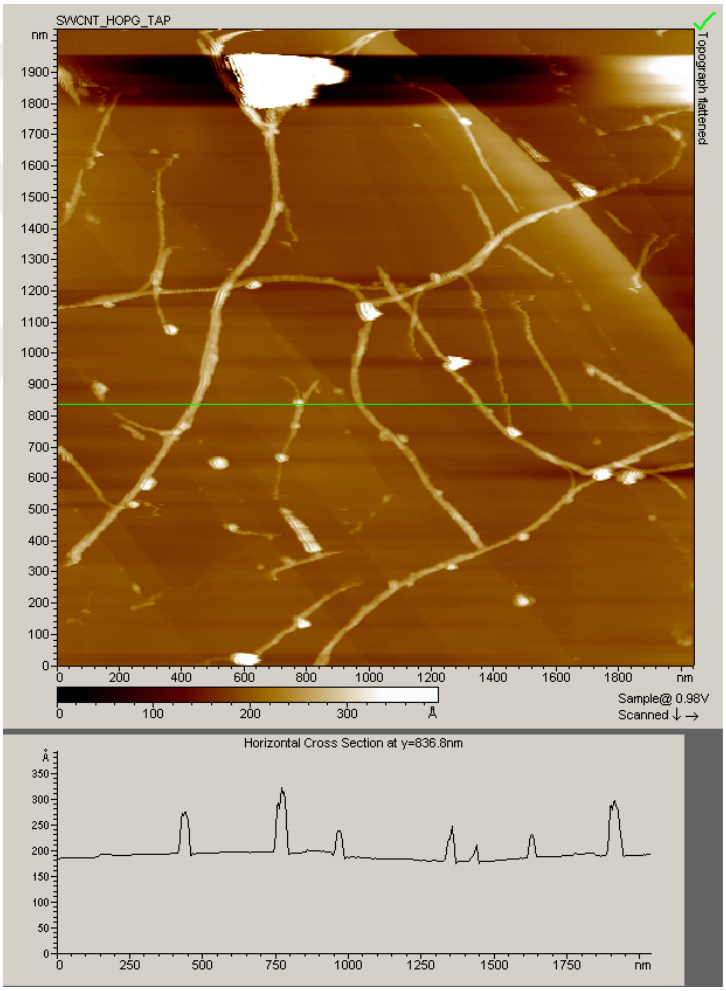

Figure 2.3 AFM tapping mode image of SWCNTs after sonication and five times dilution. Long individual features can be seen. Cross-section analysis shows that features are 10-15 nm high, suggesting that are SWCNTs are bundled.

Individual SWCNTs can be obtained by following the sample preparation method explained above. Typical large scale AFM images of individual tubes and ropes containing a number of individual SWCNTs are shown in Figure 2.4. Cross-section analysis (Figure 2.4) shows that the diameters of individual SWCNTs are around 1.2-2.5 nm, which is consistent with the literature. The AFM convolution factor affects the measured size of the tubes. As long as the tip is much sharper than the feature, the true edge profile of the feature is faithfully represented. The diameter of the AFM tapping mode tip is less than 10 nm, whereas the diameter of individual SWCNT is around 1-2 nm. Because of the convolution effect the apparent diameter of the tube is greater than its actual value.

The smallest diameter of arc-produced nitric acid treated SWCNT is expected to be 1.4 nm[10]. The AFM topography image indicates that the smallest possible diameter of individual SWCNT's diameter is around 1 nm as shown in Figure 2.4. This enables us to determine electronic density of state of individual SWCNTs by using STM.

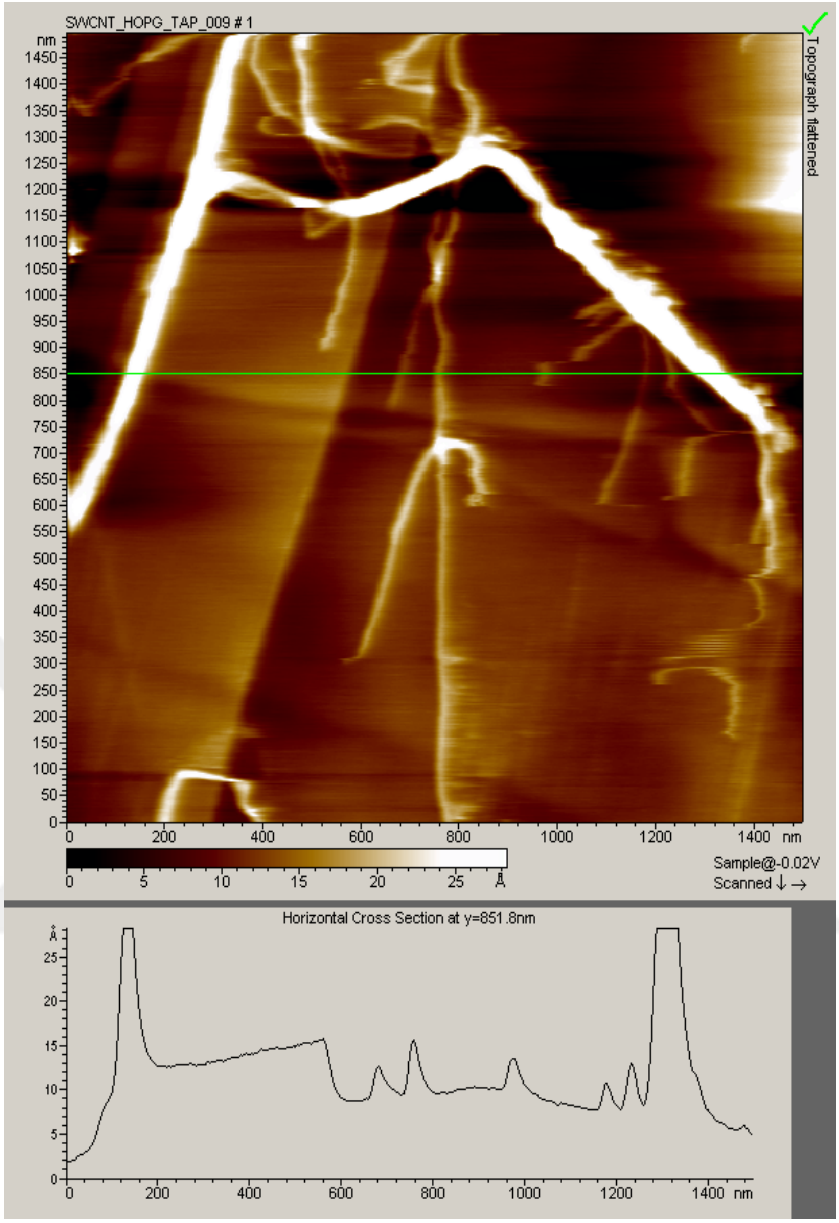

Figure 2.4 The AFM tapping mode image of SWCNTs after sonication and sixfold dilution (in ethanol) and dispersion. Cross-section analysis shows that the heights of SWCNTs are around 1.4 nm.

2.4. Electronic Density of States of Single Wall Carbon Nanotubes

The 1D band structure of SWCNTs can be constructed by 2D graphene band structure into the 1D Brillouin zone of an (n,m) SWCNT. The electronic density of states (DOS) can be computed from the band structure by summing the number of states at every energy level. The density of states is the number of available electrons per unit energy for a given energy interval. Several important characteristics of the electronic properties of SWCNTs can be obtained from the π- tight banding model. First, SWCNTs exhibit spike-like features in the DOS, which is described by van Hove singularities (VHS). Second, the DOS is zero for semiconducting tubes at the Fermi energy, but non zero for metallic tubes. Third, the VHS spacing has different characteristics relative to the Fermi energy for metallic tubes, with (3ζ-6ζ-9ζ) and semiconducting tubes, with (1ζ-2ζ-3ζ), where $\zeta=2\pi/3C_h$.

In order to study the electronic structure of individual nanotubes, current-voltage (*I-V)* curves were collected at various tip locations on the nanotubes. The curves are presented in Figures 2.6-2.12. As shown in the next paragraph, the differential conductivity dI/dV yields a measure of the surface density of states DOS. The various kinks and bumps that are seen in the experimental *I - V* curves between 0.5 and -0.5 V in Figures 2.6 and 2.8 arise from the DOS of the sample.

As discussed by Feenstra et al. (quote reference), the tunneling current I is proportional to the surface density of states $\rho(E)$ of the sample, more precisely,

$$I \propto \int_0^{eV} \exp[-2\kappa(E, eV)z]\, \rho(E) dE \qquad (6)$$

where κ is the decay length introduced in Chapter 1, and z is the tip-sample separation.

This formula implies

$$\frac{d \ln I}{d \ln V} = \frac{\rho(eV)}{\frac{1}{eV}\int_0^{eV} \rho(E) dE} \tag{7}$$

where contributions arising from the dependence of κ on *E* have been neglected. The denominator in Eq. (7) represents an averaged density of states and normalizes the numerator. Thus, curves of *d* ln *I*=*d* ln *V* have a direct interpretation in terms of the DOS. A further advantage of considering *d* ln *I*=*d* ln *V* instead of *dI*=*dV* is the the strong exponential dependence $e^{-2\kappa z}$, which masks features of the DOS, has dropped out.

The DOS of the metallic tube in Figures 2.6 and 2.8 are infinite and constant. Figure 2.9 shows an absence of electronic states, but there sharp peaks, which corresponds to the conduction and valence bands of a semiconductor SWCNT.

2.5. Demonstration of STM measurement

For conductivity measurements of SWCNT one needs to use a conductive substrate material. I preferred to use highly oriented pyrolytic graphite (HOPG) which has high conductivity and presents a flat surface. The substrate used was newly cleaved (HOPG) since large flat terraces, usually over 1μm x 1μm, can easily be found on the HOPG surface. After obtaining topographical images of SWCNT deposited on HOPG in the AFM tapping mode and determining whether or not carbon nano tubes were individual by looking at their diameter, I used the same sample in STM in order to measure the electrical conductivity of the tubes.

STM imaging studies were carried out in air and at room temperature, using electrochemically etched W tips in the constant current mode, with the bias voltage (V) applied to the tip. In order to identify SWCNTs, one needs to isolate individual tubes and look at the density of states (DOS). STS measurements were made by averaging 5-10 current versus voltage (I-V) curves at specified locations on SWNTs. The STM image shows both individual and bundled SWCNTs in Figure 2.5. The first experiments that directly addressed these theoretical predictions were done by Odom and Wildoer using low-temperature STM[9]. These initial STM studies characterized the atomic structures and electronic density of states. Odom and Wildoer confirmed the existence of both metallic and semiconducting SWCNTs for a wide range of structures. The individual SWCNTs corresponding to the tip positions A and D in Figure 2.5 indicate metallic and semiconducting behavior with STS as shown in Figure 2.5, respectively.

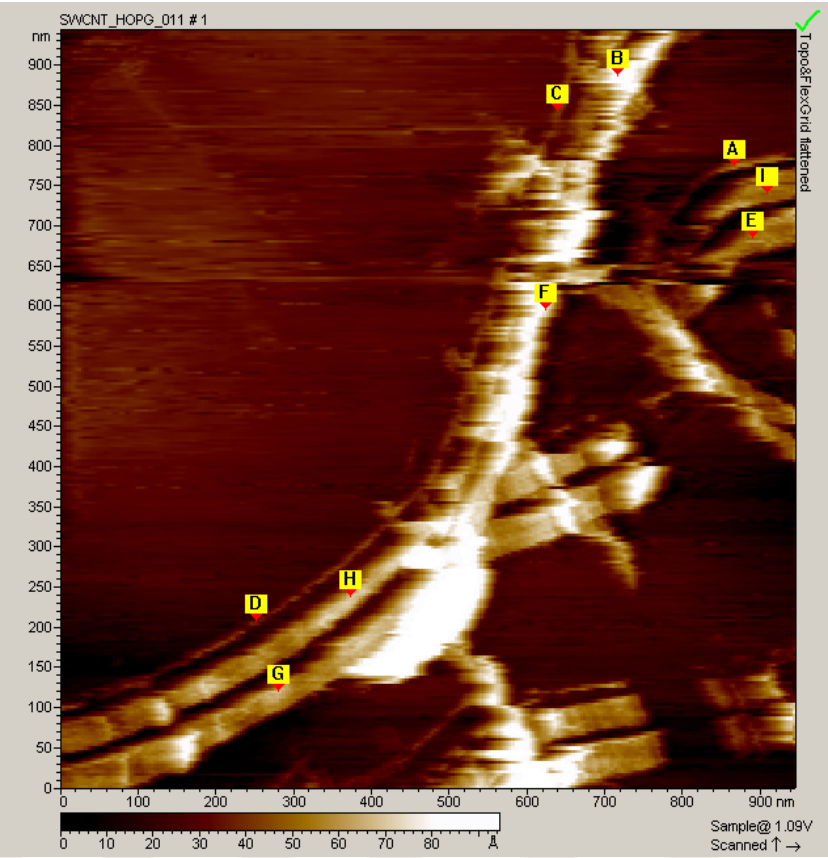

Figure 2.5 STM constant current mode images of SWCNT after sixfold dilution and dispersion. Two individual and bundled SWCNTs are seen in the image. STM tip is located in different locations on the tubes in order to determine I-V curves. The individual SWCNT located in position A has diameter around 1.8 nm and it shows semiconductor behavior as shown in Figure 2.9. In D position the other individual SWCNT is shown with metallic behavior as shown in Figures 2.6 and 2.8.

The scanning tunneling spectroscopy shows that the DOS is nonzero for metallic SWCNT at Fermi energy level, but zero for semiconducting tubes, as shown in Figure 2.9.

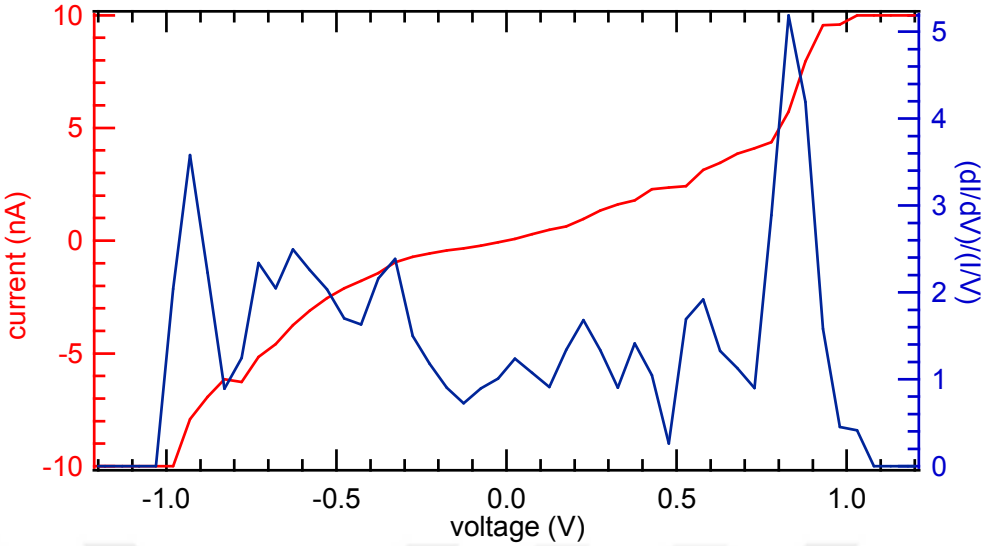

Figure 2.6 The density of states of SWCNTs for semiconducting tube. The inset shows that the normalized conductance DOS, indicated in blue, is not zero at the Fermi energy.

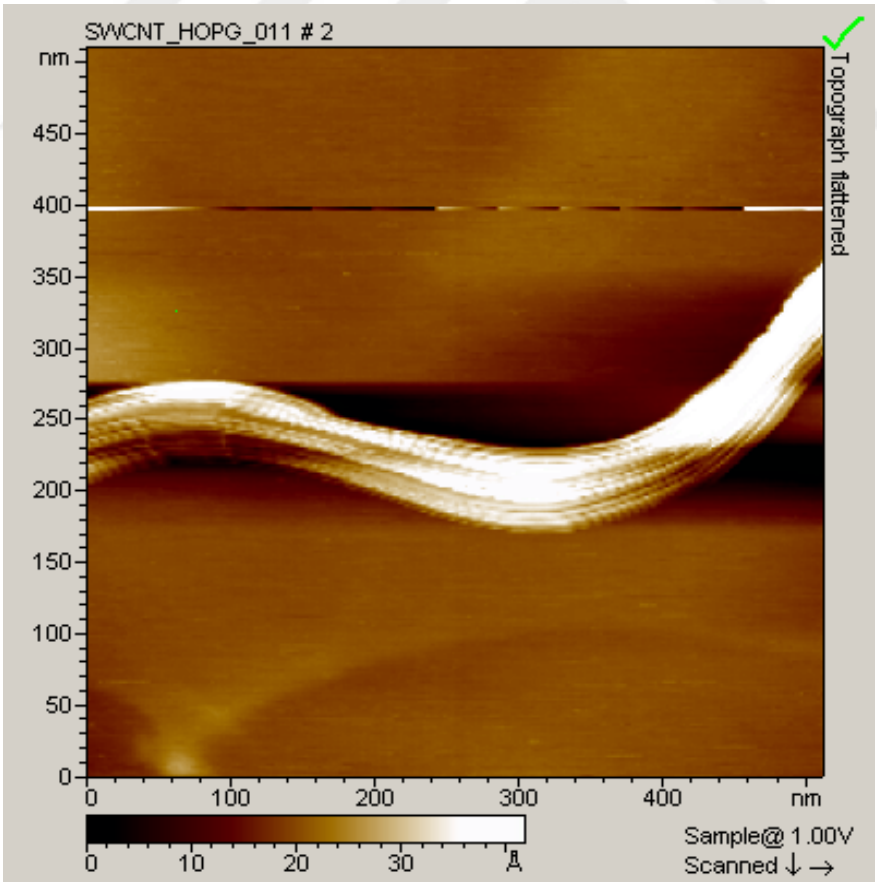

Figure 2.7 STM image of bundled of SWCNT with the diameter~ 50nm.

2.5.1. Spectroscopic Measurements of SWCNTs

Spectroscopic measurements by STM consist essentially of bringing the STM tip 5-15 Å away from a sample surface, applying a voltage between the tip and the sample, and measuring the resulting tunneling current at different locations on the SWCNTs. The applied voltage raises the Fermi energy of the sample with respect to the Fermi energy of the tip. Electrons with an energy below the Fermi level in the sample but above the Fermi level in the tip tunnel from the sample through the unoccupied state in tip. When the voltage is increased, more and more electrons have sufficient energy for tunneling.

The current – voltage (I-V) curves were obtained by placing the tip on different locations on the nanotubes in the STM feedback loop. The (I-V) curves are presented in Figures 2.6-2.12. The differential conductivity dI/dV yields a measure of the surface density of states DOS. The various kinks and bumps that are seen in the experimental I-V curves between -0.5 and 0.5 V in Figures 2.6 and 2.8 arise from the DOS of the sample. The first step in an analysis of these features is to compute the derivative, dI/dV, shown together with the I-V curves in Figures 2.6-2.12. The derivative highlights the DOS features; however, it also varies exponentially in voltage and tip sample separation[11]. This variation causes to masks the relevant DOS features. To eliminate this problem, we normalize dI/dV by the conductance of the junction. We compute the ratio of differential to total conductivity (dI/dV)/ (I/V)≈ d(ln I)/d(ln V) which provides a good measure of the density of states shown in Figures 2.6-2.12. Notice that, the DOS of the metallic tube in Figures 2.6 and 2.8 is finite and constant. Figure 2.9 shows an absence of electronic states, but there are

sharp peaks, which correspond to the conduction and valence bands of a semiconductor SWCNT.

The measurement of electronic properties of SWCNTs were measured before by T.W. Odom (2001) by using ultra high vacuum STM (UHV-STM) with laser vaporized SWCNT deposited on Au(111). They reported that the normalized conductance (V/I) dI/dV provides a good measure of major features in the local density of electronic states (LDOS) for metals and semiconductors[12].

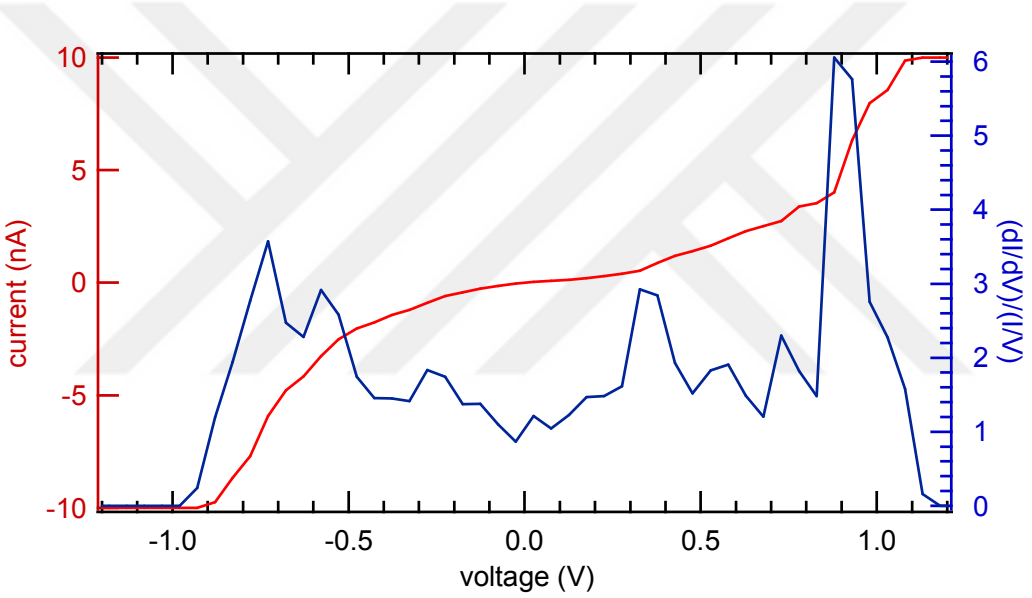

Figure 2.8 The STM image of SWCNT. DOS of individual metallic SWCNT is shown. I-V curve shows a low conductance at a low bias.

The electronic properties of single-walled carbon nanotubes are shown in Figure 2.8. The current–voltage curves were obtained from tunneling spectroscopy on individual nanotubes. The normalized conductance (dI/dV)/(I/V) was calculated from I-V curves recorded at several positions on the tube in the inset. The inset shows a constant current image of the semiconducting nanotube. The electronic density of states of SWCNT was obtained by calculating the first derivative of the current with

respect to the voltage and dividing the first derivative of the current by the all total conductivity of substrate.

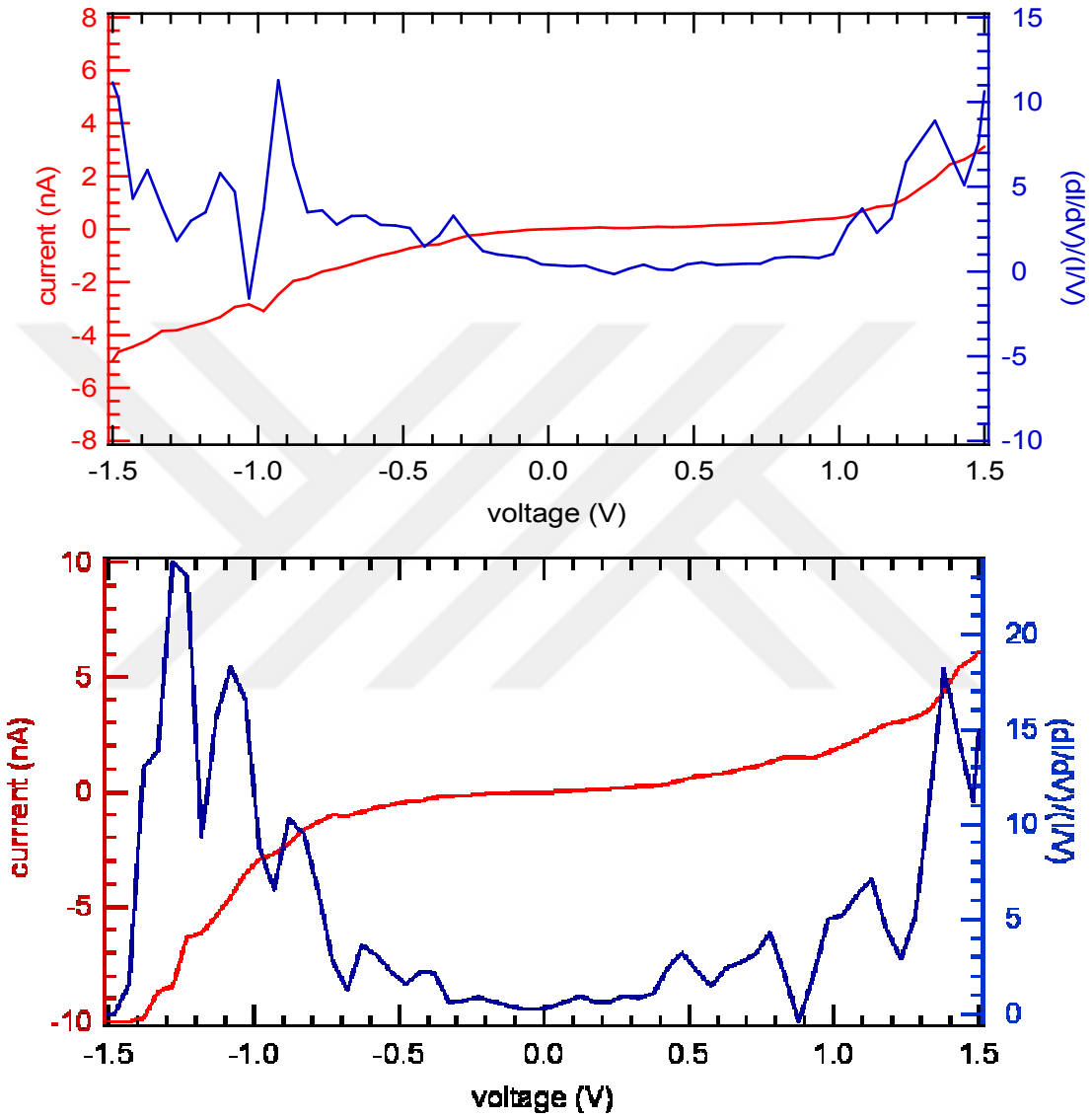

Figure 2.9 The Scanning Tunneling Spectroscopy of SWCNT. The I-V curve of individual semiconducting SWCNT is shown in red, and normalized conductance of individual semiconducting SWCNTs is shown in blue.

Electronic transitions between the energy bands of SWCNTs can be observed by standard spectroscopic measurement[13]. The energy differences between the valence

band and the conductance band is about 0.7 eV for semiconducting arc produced SWCNT[14], as is consistent with the Figure 2.9. The band gaps are inversely proportional to the tube diameters[15].

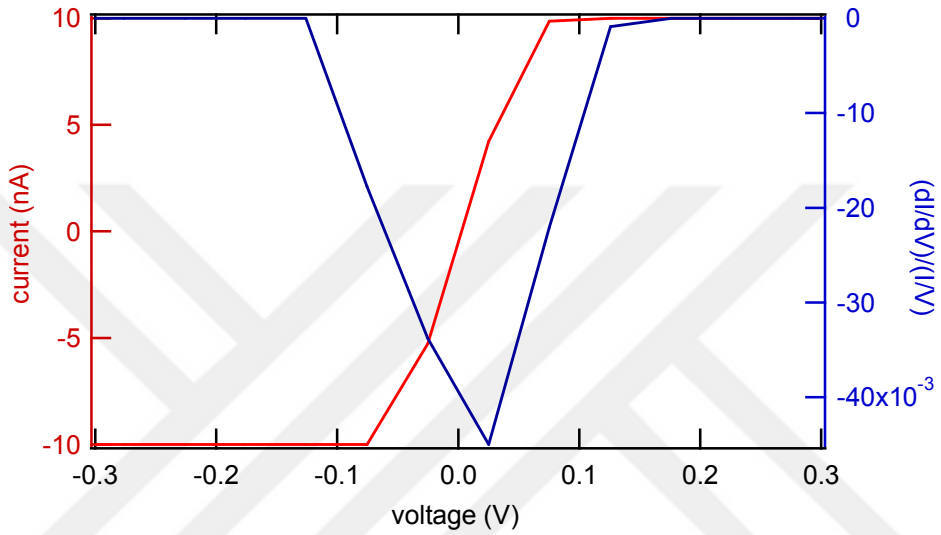

Figure 2.10 Increasing in voltage increases the current by following the Ohm's Law as shown by red color.

The electronic DOS of SWCNT has a very sharp dip around the Fermi level. According to Quyang, the reason for sharp dip is that the SWCNT is located on a bundle of SWCNTs.

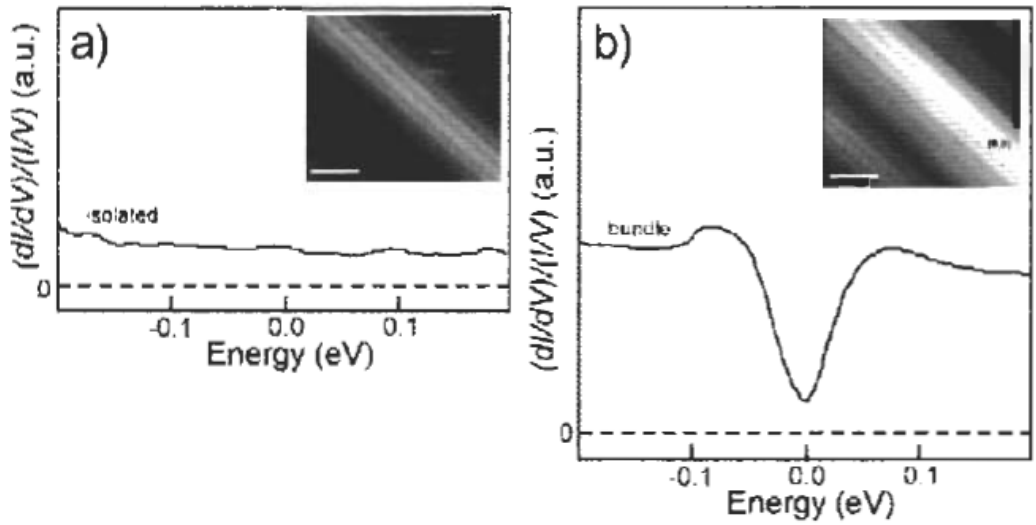

Figure 2.11 a) Low-energy density of electronic states in an isolated (8, 8) nanotubes. The inset shows an STM picture of the tube. b) Density of electronic states for an (8, 8) tube on the top of a nanotubes bundle. The inset shows the (8, 8) nanotubes on the top of a bundle. The calculated DOS for an isolated (8, 8) tube is displayed below the atomic resolution os SWCNT. Typical high-resolution $(dI/dV)/(I/V)$ and measured *I-V* data in the low-energy region [16].

Quyang measured the low energy density of state of an isolated (8, 8) nanotubes and an (8, 8) nanotubes on top of a bundle, as shown in Figure 2.7, which shows as STM image. STM image of isolated (8, 8) SWNTs on Au (111) substrate, recorded in constant-current mode with a bias voltage of 0.55 V and a tunneling current of 0.10 nA. The scale bar, 1 nm and dI/dV was recorded on (8, 8) armchair SWNTs[16]. In the isolated case the DOS is constant around Fermi level as shown in Figure 2.7 for the (8, 8) nanotubes. In the vicinity of a bundle, a sharp dip is found in the electronic DOS, as shown in Figure 2.10.

Another reason for the sharp dip around the Fermi energy level can be the low resistance contact with sample. Dekker reported electrical transport measurements of

individual nanotubes using low-resistance contacts (LRCs). An electric field is established across the nanotubes which accelerates electrons by applying a bias voltage between two LRCs, which leads transport of high energy electrons[17].

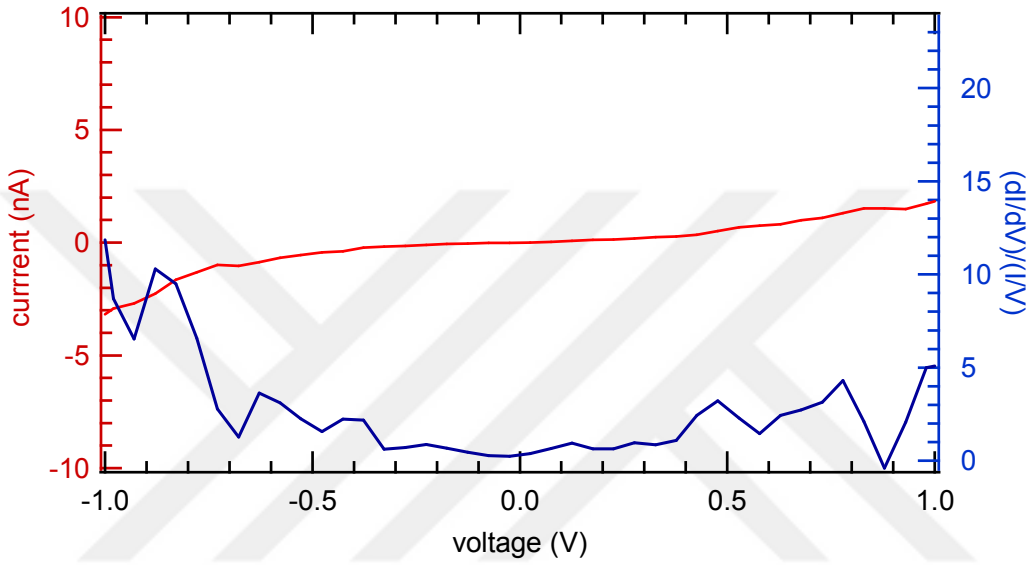

Figure 2.12 The STM image of SWCNT. The individual tube tip positions in D and A corresponds to metallic and semiconducting individual SWCNTs, respectively. a) The I-V curve of metallic SWCNT is shown. b) I-V curve of SWCNT is shown in red, and the DOS of states of individual semiconducting SWCNTs in blue.

The electronic properties of single-walled carbon nanotubes are shown in Figure 2.12. Current–voltage curves obtained from tunnelling spectroscopy on various individual nanotubes and normalized conductance (dI/dV)/(I/V) curves calculated from I-V curves recorded at several positions on the tube. The inset shows a constant current image of the semiconducting nanotube. The curve shows a low conductance at a low bias. Those data are consistent with the results of T.W. Odom 1998[18].

2.5.2. Demonstration of UV visible Near Infrared Raman Spectroscopy

The transition between the energy bands of SWCNTs can be observed by UV visible spectroscopy [19, 20]. Near-infrared spectroscopy has become an important tool for characterization of the electronic band structure of SWCNTs[13, 21] . Present methods of synthesis produce SWCNTs with a range of chiralities and diameters, and this yields mixtures of metallic and semiconducting SWCNTs[22]. The semiconducting SWCNTs show a series of transitions between the principal mirror spikes in the DOS. The transitions for semiconducting SWCNT are given by $S_{11} = 2\alpha\beta/d$ and $S_{22} = 4\alpha\beta/d$, whereas the metallic SWCNTs show the first transition at $M_{11} = 6\alpha\beta/d$. The coefficient α is the carbon-carbon bond length (nm), β is the transfer integral between $p\pi$ orbitals, and d is the diameter in nm[21-23]. In figure the S_{22} transition occurs at 1.25 eV, so the S_{11} transition will be $S_{22}=2S_{11}$ which is 0.625 eV. This result shows that band gap is shifted ~0.1 eV compared to the DOS spectra shown in Figure 2.13. The usa of nitric acid in purification of the SWCNTs leads to partial exfoliation and intercalation in graphene as a hole dopant. After purification of SWCNT by nitric acid, the valence band of semiconducting tubes is partially depleted due to oxidation. The decrease in intensity and the shift of optical transition between the first pair of Van-Hove singularities in the DOS to higher energies can be explained by doping effects[24].

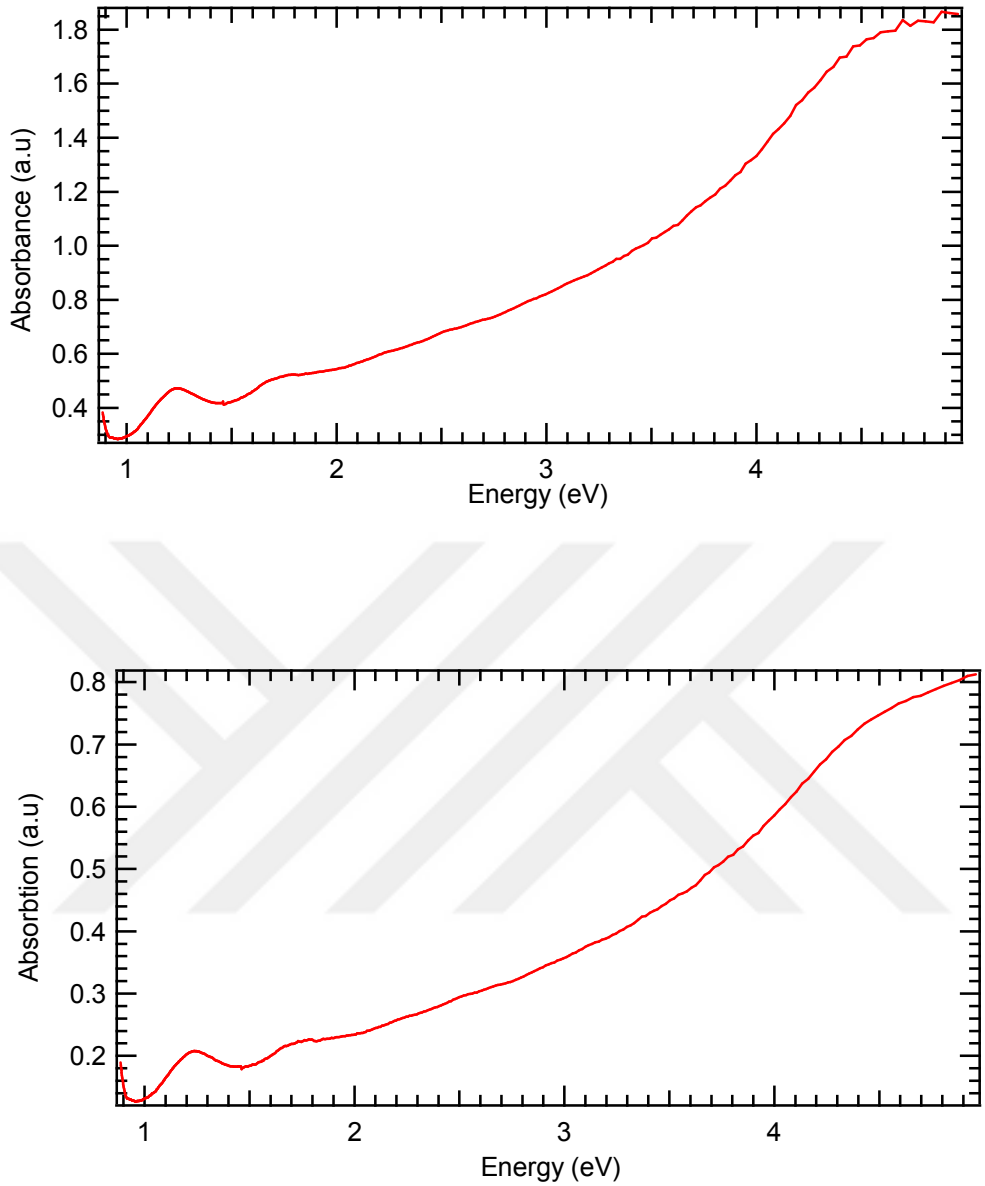

Figure 2.13 The UV- Near IR spectroscopy of SWCNT. The spectrum shows that the S_{22} tranmission energy is about 1.25 eV for different consantrated solution of SWCNT and ethanol.

The UV-Near IR spectroscopy shows we have purified carbon nanotubes in our solution by looking at the absorbtion energy.

CHAPTER 3

3. History of Near-field Scanning of Optical Microscopy (NSOM)

Leeuwenhoek used a single-lens microscope to make the first observations of bacteria and single cells in the late seventeenth century[25].

The microscope is the most important tool for research in the biological sciences. As technology has progressed, allowing for better resolution, microscopes have been used to study the observation of smaller and more complex samples. The optical microscope is often said to be the most successful scientific instrument in history. During the twentieth century, optical microscopy lagged behind of newer techniques such as transmission electron microscopy and scanning tunneling microscopy. The resolution of optical microscopy has stopped progressing, as modern fabrication techniques produce the ultimate resolution allowed by the diffraction limit.

In the early 1870s, Ernst Abbe formulated a rigorous criterion for being able to resolving two objects in an optical microscope:

$$d > \lambda / (2\sin\theta)$$

where d = the distance between the two objects, λ = the wavelength of the incident light, and 2θ = the angle through which the light is collected [26]. To improve optical resolution, this criterion suggests that one only need use light of shorter wavelength.

Recent developments in nano-technology have allowed one to overcome this diffraction limit. The invention of the near–field scanning optical microscopy (NSOM) followed scanning tunneling microscopy (STM) and atomic force microscopy (AFM). It leads to the development of advanced nano-optic devices and a broad range of applications of optical spectroscopy to the nanometer-scale world.

The goal of overcoming the limitations of far field optics (the oldest form of microscopy) and greatly improve optical resolution has led to the development of near-field scanning optical microscopy (NSOM). The development of NSOM scanned probe microscopy began in the early part of twentieth century. The first idea about NSOM was by Synge in 1928-1932. Synge proposed that "you could distinguish two particles separated with distance of sub-wavelength by illumination of one spot through a small pin hole punched in a metal plate which was placed at the near-field region of the particles." After Synge, other scientists developed image acquisition techniques which we use today. The ultimate resolution has been obtained by aperture NSOM around 10 nm. Researchers wanted to image objects optically at smaller and smaller scales. In order to do that, one needed to be bring the tip closer to the surface at a distance less than the wavelength of light. However, this involves some difficulties and limitations. Because of the rigorous dimensional requirements for both aperture size and probe-sample separation, visible light NSOM experiment did not appear in the literature until the early 1980s, paralleling the development of other scanned-probe microscopes. Although its development was distinct from these other methods, NSOM uses similar instrumentation for controlling the tip and sample motions. The scanned-probe technology developed in this era was incorporated into NSOM methods, leading to the explosive growth of near-field microscopy. With

NSOM the spatial resolution was of the order of 100 nm[27]. Looking for even better resolution has lead to ANSOM, which has achieved 10 nm[28, 29].

3.1. Introduction to Near- Field Scanning Optical Microscopy (NSOM)

Near-Field Scanning Optical Microscopy (NSOM) aims at optically resolving sub-wavelength structures. The most common form relies on the local excitations of the sample surface by the optical fields. The earliest discussion of near-field optical microscopy appeared as early as 1928, when Synge suggested the illumination of samples through an aperture[30, 31]. He described how optical imaging could be performed so that the spatial resolution would no longer be limited by diffraction phenomena. He used a tiny light source formed from a sub-wavelength size aperture in a conducting metal screen. The microscope Synge proposed is shown in Figure 3.1. The field that is laterally confined to a cross sectional area is determined by the aperture dimensions with the light on the back side of the aperture. Field confinements occur only within a distance of about one aperture diameter from the hole and it is restricted to the region known as the near field. When the sample is held in near field region, only the sample surface directly beneath the aperture is illuminated. Hence, the optical properties of sub-wavelength-size sample regions can be directly probed. The spatial resolution of NSOM images are limited by the size of the aperture and its distance from the sample, rather than the wavelength of light employed[32].

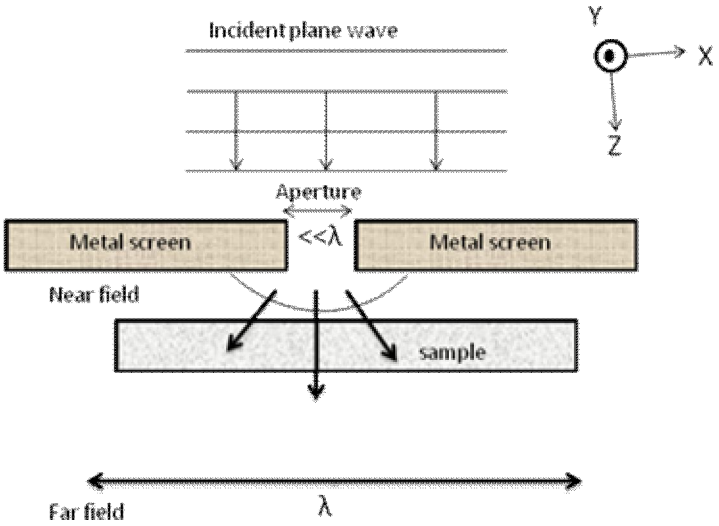

Figure 3.1 A simple model for the aperture-based near-field optical microscope. A sub-wavelength-size aperture is produced. The screen and aperture are shown in cross section[33].

Scanning near field optical microscopy (NSOM) has four modes of operation, as shown in Figure 3.2:

- Transmission mode imaging: Illuminating the sample from underneath with an inverted microscope and collecting the transmission by the NSOM aperture.
- Reflection mode imaging: By using external objectives, the reflected light is collected from the sample surface.
- Collection mode imaging: The back reflected signal from sample surface is collected by the aperture while the sample is illuminated with a light source from the top or bottom.
- Illumination/collection mode imaging: The sample is illuminated by the SNOM aperture, and the transmitted radiation through the sample is collected, as suggested in the original idea of Synge, using an inverted optical microscopy.

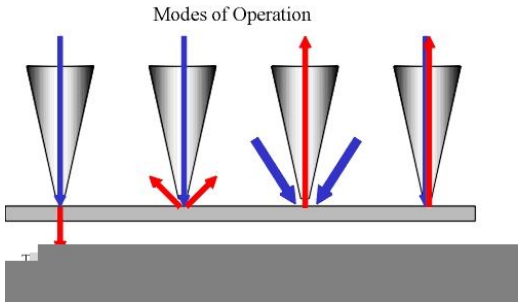

Figure 3.2 Transmission, reflection, collection, and illumination modes from left to right, respectively[34].

3.2. Introduction to Apertureless Near-field Scanning Optical Microscopy (ANSOM)

ANSOM is apertureless near field scanning optical microscopy, also known as scattering type scanning near-field optical microscopy (sSNOM). ANSOM employs a metalized tip instead of an optical fiber probe (Innouye 1999, Anderson 2000, and Hamann 2000). In ANSOM the tip illuminated by an external source, scans the surface, while light scattered from the tip is collected. ANSOM reduces the detected background signal either by homodyne or heterodyne detection by demodulating the signal in higher harmonics of the frequency of tip in order to obtain high resolution of order 10 nm or better[28, 35].

A small dimension tip (metallic or dielectric) which is smaller than the wavelength of light is brought in close proximity to the sample surface. When a laser source focuses onto the AFM probe, the AFM tip scatters light and enhances the electric field, owing the strong interaction between evanescent field and probe, as shown in Figure 3.3. The scattered light consist of two parts; one of them is the near field, that comes from

a very small vicinity of tip apex and the second part is the far field, which contains parasitic signals from the tip body and the sample surface.

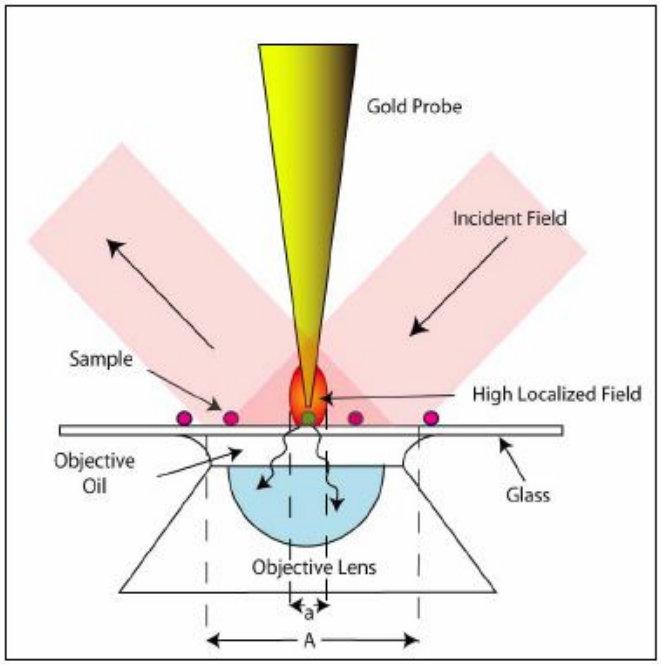

Figure3.3 The demonstration of localized field around tip and surface in apertureless type of NSOM[36].

In order to excite a periodic vibration of the apertureless tip, the diffraction spot of a laser beam is focused onto the sample. A dither motion is simultaneously applied to the sample at different frequencies in a direction perpendicular to the sample surface. When the tip is positioned on the sample, it generates a much greater and a more local perturbation of the field. Once the tip reaches the surface, its vibration amplitude suddenly decreases and becomes proportional to the tip-sample average distance. As the tip vibrates perpendicularly to the sample surface with this

amplitude, it slightly perturbs the surface plasmon polaritons (SPPs) in metals, and the incident light field on the sample is enhanced strongly[37].

A collective oscillation of electrons or a plasma wave near the surface of a metal is known as a surface Plasmon. The surface plasmon polariton can be excited by irradiation with an evanescent light wave. A sharp metallic tip plays an important role in the localized field enhancement, which is attributed to surface plasmon polaritons (SPPs) locally confined in the close vicinity of the tip apex.

3.2.1 Early Developments of ANSOM

Various modulation methods have been proposed for apertureless NSOM. In the original proposal by Zenhausern and Wickramasinghe's team involves the subwavelength-sized AFM probe introduces a short-range perturbation of an optical field [38]. The perturbation is detected, and its magnitude used to form an image, by achieving 5 nm resolution in 1994[38-40].

A second apertureless technique, based on the periodic occlusion of an illuminating beam by a sharp metallic probe, was proposed by Boccara's group in 1995 [41-43]. This approach has not been pursued, since the achieved resolution was disappointed.

Kawata proposed a third technique, called frustrated total-internal-reflection near-filed microscopy in 1995. Kawata's set up consists of using a tapping AFM probe to locally perturb the optical evanescent field at a glass-air interface above a prism [44, 45].

3.2.2. ANSOM Probes

The performance of ANSOM depends on the electric field enhancement factor of the metalized tip. A metal coated AFM tip fabricated by the sputtering method is usually used as the ANSOM probe. The cancellation of the electric field component along the tip axis and the rounded tip effect decreases the electric field enhancement factor[46]. In order to overcome this problem, one needs to polarize the electric field along the tip axis and increase the signal-to-noise ratio[47].

The shape of the ANSOM tip has an important function in obtaining high spatial resolution. Any commercially available non-contact AFM tip is suitable for the ANSOM[44]. The important property of ANSOM tip is the geometrical accessibility of the tip apex for illumination [48]. Theoretically, the exciting optical field should be centered at the tip apex in order to collect signal from the tip body and the sample surface.

Silicon and metallic tip

In ANSOM, in order to generate light in a nano-scale region, the light needs to be illuminated onto both tip and the sample by using external optics, such as lenses, mirror, etc. In this case, the diffraction limited spot focused onto the sample generates background fluorescence. This back ground signal is comparable to the tip-enhanced near field fluorescence. In order to solve this problem, several groups have proposed the use of silicon tips[38, 44, 49]. According to their results, the silicon tip

reduces the quenching; however, at the same time the field enhancement is diminished, resulting in a large back ground signal.

Ogawa achieved 15 nm resolutions both on quantum dots and single dye molecules by using a silicon tip[50].

Metallic ANSOM probe provides high electric field efficiency. On the other hand, silicon tips can be used to overcome the two major drawbacks of near field fluorescence detection, which are quenching and background signals[51]. The silicon tip allows for quenching-free detection, while two photon excitation schemes enhance the scattering rate near the tip apex. Thus the fluorescence signal from this tiny volume outweighs the one from diffraction limited focal spot. Abe performed tip-enhanced two photon excited fluorescence microscopy using a silicon tip. He demonstrated that individual quantum dots can be clearly resolved with spatial separation of 70 nm, as shown in Figure 3.4 [51].

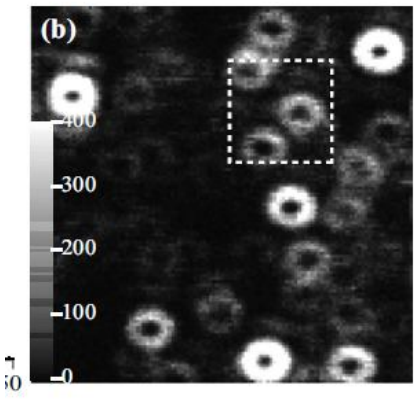

Figure 3.4 Zoomed two-photon excited fluorescence image of quantum dots obtained with azimuthally polarized silicon tip[51].

The three ring quantum dots shown in Figure 3.4 were observed when the sample was scanned with a silicon tip aligned in the longitudinal direction. Since the tip-enhancement is induced by the longitudinal field component of the electric field within the tightly focused spot[52], it was possible to achieve high spatial resolution.

3.2.3. Advantages and Disadvantages of ANSOM

Most of the instruments built for scanning optical near-field microscopy (SNOM) use a metal coated tapered optical fiber with a nanometric hole at the tip apex (Lewis 2 et al. and Pohl et al.3). This set up can be used as a nanosource, which illuminates a small region of the sample surface, or as a nanodetector, which collects the local electromagnetic field of the sample irradiated by a far-field source. High spatial resolution requires a nanometer-sized aperture in NSOM. A metal coated optical fiber tip is used in order to direct or collect the light from the sample. However, due to the propagation cut off of the waveguide mode in fibers, only a small fraction of the light can be transmitted through the tip[53]. This makes some difficulties in using such a probe in lithographic applications.

The higher resolution requires the smaller aperture to get smaller signal from the background. Since most NSOM uses tapered single mode optical fibers coated on the sides with a metal substance, the smallest aperture is not easy to achieve. A problem with using a metal coated fiber is the skin depth of the metal. For example, the skin depth of aluminum is 12 nm at 633 wavelengths. When aluminum is used to

confine the light within the optical fiber as it enters the tip the smallest aperture cannot be much smaller than twice the optical skin depth in aluminum[54].

Other drawbacks of ANSOM are fluorescence quenching by the metallic tip and background signals from the diffraction limited focal spot when a metallic probe is used.

Apertureless near-field scanning optical microscopy (ANSOM) has overcome this problem by using sharp metallic tips instead of fiber apertures to achieve nanometer-scale resolution.

Near-field scanning microscopy (NSOM) relies on a Tip-to-Sample Gap (TSG) which depends on the tip aperture size. ANSOM has some advantages over NSOM, such as high spatial resolution, tolerance to high-density electro-magnetic power. The TSG is maintained by monitoring a laser beam reflected from the back side of the tip into a quadrant detector in AFM.

Apertureless NSOM has four advantages over aperture NSOM.

1) Higher optical resolution can be obtained with ANSOM. This is because the field enhancement occurs in a much more localized area of the tip,with suitable incident field polarization[55].

2) The problem of the strong attenuation in the fiber in NSOM is diminished in ANSOM since the light is focused onto the tip from the far field without loss. In NSOM the loss is higher than in ANSOM[55].

3) Apertureless NSOM tips are more robust, and their fabrication is more reproducible than optical fiber tips. In ANSOM any kind of commercial AFM tip can be used[54, 56].

4) The range of useable wavelengths is not limited. ANSOM can be performed with IR-Raman and Fluorescence NSOM wavelengths[57].

On the other hand, ANSOM has some disadvantages compared with NSOM. The main disadvantage of ANSOM comes from the strong scattered light at the tip shaft and in the far field. Furthermore, the background varies during scanning because of the z-motion of cantilever. However, this is not a serious problem anymore, due to some successful strategies [58].

An important advantage of NSOM is the negligible background signal. With a perfect metal coated aperture the only scattered light comes from the sub-wavelength aperture.

3.2. ANSOM set up

Tapping mode AFM is the better choice for ANSOM since the oscillation amplitude and the tip-sample distance can be controlled. In addition, the linear distance-amplitude dependence allows the distance between the sample and average position of tip to be easily stabilized at a constant value during scanning. It is important to avoid touching the sample surface with the tip, since it induces some undesired higher harmonics. This prevents damage to tip and the sample. The output signal of the

feedback loop provides a topographic image of sample. Shear forces on the tip and their destructive influence are almost eliminated in tapping mode[48]. For these reasons the tapping mode is preferable.

A typical ANSOM setup consisting of optical components, an external laser source, and a sample stage is shown in Figure 3.5.

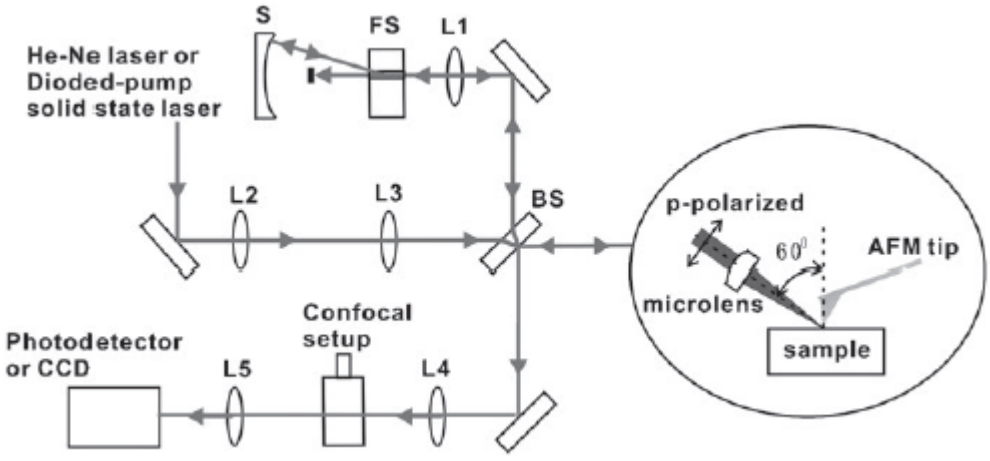

Figure 3.5 Schematic layout of multi-wavelength scattering-type scanning near-field optical microscope. FS: frequency shifter; S: spherical mirror; BS: broadband beam splitters L1–L5: lenses.

Figure 3.5 shows the configuration of the system which Gomez developed. A P-polarized laser illuminates the sample from above with incident angle 60 degrees to achieve dark-field illumination. The evanescent field generated over the sample surface is scattered by the AFM tip. By using the same optics, the scattered light is collected. The image of the scattered evanescent field was taken by a CCD camera as shown in Figure 3.6. The very small area of light is seen on the tip of the probe. The size of this area is much smaller than the radius of tip (Yasushi Inouye).

The imaging of the surface of the sample in the tapping mode was performed simultaneously with the detection of the scattered light. A photo-detector was placed near the probe to collect light scattered at a small angle to the surface of the sample in the direction opposite to the incident beam. The electrical signal from the detector was amplified by a lock in amplifier at the frequency of the cantilever oscillation and collected by a computer simultaneously with AFM data. The use of an oscillating cantilever eliminates the DC background signal and provides the benefits of sensitive lock-in detection [59].

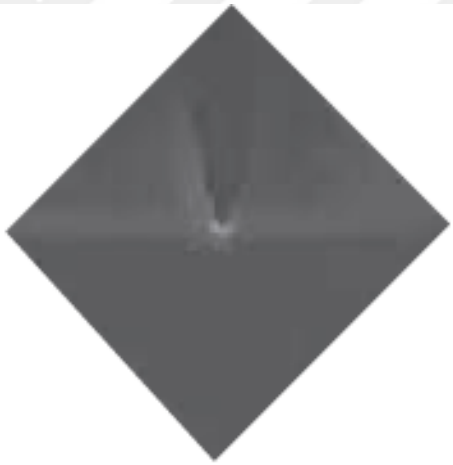

Figure 3.6 Enhanced electric-field intensity localized at a silver probe tip, calculated by the FDTD method[60]

Scattered light leads to unwanted background scattering from the tip of the body or sample surface. Since the background signal suppress the near field signal, a lock in detection technique can be applied for tip-enhanced signals in order to separate the near field signal from the background signal by increasing the signal-to-ratio of the

near-field signal. By vibrating the probe tip along the z axis, at a certain frequency and with nanometric amplitudes, and demodulating this signal with a lock-in detection technique, the scattered evanescent signal can be recovered[60, 61]. The intensity distribution of the light field decays rapidly along the z axis, so that the scattered evanescent field is recovered. On the other hand, the intensity of the non-evanescent waves does not decay at sub-nanometric resolution. As a result, unwanted contributions from scattered non-evanescent photons are eliminated in the measured signal. Inouye's Group performed an experiment to measure the exponential decay of the evanescent field produced by the total internal reflection with this NSOM[61].

CHAPTER 4

4. Tip - Near Field Enhancement and Data Acquisition

4.1. Field Enhancement

The field near a sharp metallic tip can be strongly enhanced if radiated with an optical field polarized along the tip axis. The enhancement has its origin in the electrostatic lightening rod effect. The lightening rod effect is due to the geometric singularity of sharply pointed structures and localized surface plasmon resonances. Novotny (2003) demonstrated that second harmonic generation leads to field enhancement near a sharp tip[62].

The central to ANSOM is the scattering of the evanescent field localized around the tip due to the sample structure or vice versa. The apex of a metallic probe functions as a scatterer by enhancing the electric field locally. Shown in Figure 4.1 is the intensity of a light field scattered at a tip. When the tip is placed in contact with a substrate, the tip is illuminated by the plane wave traveling from the substrate. As long as the angle of the incident light satisfies the condition of total internal reflection, an evanescent field is generated over the surface. A localized and enhanced field spot is observed around the tip in Figure 4.1. The size of the small spot corresponds to the radius of tip. The enhancement of the electric field is much stronger when TM (p-

polarization) is used for illumination. No enhancement of the electric field is induced, when TE (s-polarization) is used for illumination. The material for an apertureless probe can be a semiconductor or a dielectric; however, in order to get strong enhanced field, one needs to use a metallic tip and TM mode illumination.

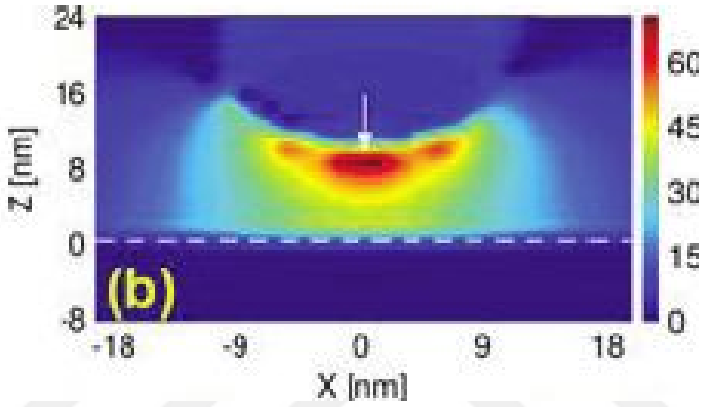

Figure 4.1 Field enhancement of light the arrow indicates the apex of the Au tip[63].

A structure of an apertureless probe tip is expressed by $\boldsymbol{P}(\boldsymbol{r})$;

$$\boldsymbol{P}(\boldsymbol{r}) = \int \boldsymbol{P}'\left(\boldsymbol{K}_{\boldsymbol{prob}}\right)\boldsymbol{exp}(\boldsymbol{iK}_{\boldsymbol{prob}}.\boldsymbol{r})\boldsymbol{dK}_{\boldsymbol{prob}} \tag{8}$$

where $\boldsymbol{P}'(\boldsymbol{K}_{\text{prob}})$ is the spatial spectrum of the tip according to scalar theory[60].

When an incident light field, whose wave vector is represented by $\boldsymbol{k}_{\text{inc}}$ is scattered by the tip, the scattered field is given by

$$\int \boldsymbol{P}'\left(\boldsymbol{K}_{\boldsymbol{prob}}\right)\boldsymbol{exp}[\boldsymbol{i}(\boldsymbol{K}_{\boldsymbol{prob}} - \boldsymbol{k}_{\boldsymbol{inc}}).\boldsymbol{r}]\boldsymbol{dK}_{\boldsymbol{prob}} \tag{9}$$

The scattered field, of which the wave vector $|\mathbf{K}_{prob} - \mathbf{k}_{inc}|_\infty$ is imaginary, is converted into an evanescent field and is localized around the tip as shown in Figure 4.1. $|\mathbf{K}_{prob} - \mathbf{k}_{inc}|_\infty$ is equal to $|\mathbf{K}_{prob}|_\infty$, that is, $|\mathbf{k}_{inc}|_\infty$ is negligible if the tip apex is much smaller than wavelength of the light field. This means that the size of the small light spot is approximately equal to the tip radius.

A sample with structure smaller than the wavelength is described similarly by

$$\boldsymbol{S}(\boldsymbol{r}) = \int \boldsymbol{S}'(\boldsymbol{K_{str}})\boldsymbol{exp}[\boldsymbol{iK_{str}}.\boldsymbol{r}]\boldsymbol{dK_{str}} \tag{10}$$

where $\boldsymbol{S}(\boldsymbol{K}_{\mathbf{str}})$ is the spatial spectrum of the sample. The small spot around the tip is scattered by the sample when it is placed in the vicinity of the tip. To convert the scattered field into a propagating field, lateral component of the spatial spectrum must satisfy the condition.

$$\left|(\boldsymbol{K_{prob}})\infty - (\boldsymbol{K_{str}})\infty\right| < \frac{\boldsymbol{w}}{\boldsymbol{c}} = \frac{\boldsymbol{2\pi}}{\boldsymbol{\lambda}} \tag{11}$$

According to this criterion, Eq. (11) represents that the evanescent field around tip is scattered by the sample whose spatial frequency is almost same as the wave number of the evanescent field. It means that if you want to get certain resolution on nm scale, you should use a probe with that nm scale since the tip functions as a spatial band filter. The smaller radius probe gives the higher spatial resolution, as the tip converts evanescent fields of higher spatial frequency into a propagating field[60, 64].

4.2. Signal Detection

4.2.1. Lock-in detection

Lock-in detection is frequently used to increase the signal-to-noise ratio of weak signals obscured by relatively strong background noise. Typically, one uses time-harmonic modulation of some experimental parameter and filters the observable quantity at the same quantity. Filtering at higher harmonics of the modulation frequency yields additional information, whose exact nature depends on the particular setup.

In order to detect a weak near field signal with an intensive background noise, lock in signal detection technique can be used[65, 66]. In the lock-in light detection method, a signal light modulated at a frequency f is incident on a photo-detector together with a background light. An output signal from the PMT is fed into a narrow band-pass filter whose center frequency is tuned at the frequency f and then fed into a multiplier. For the multiplier, a reference signal with the same frequency f as the modulation frequency of the signal light is also supplied. The multiplier circuit works essentially as a signal sampling gate with a duty ratio of 50%. The timing of the reference signal is adjusted to be in phase with that of the output signal from the PMT by a phase delay circuit. Finally, the direct-current (dc) level signal is obtained through a low-pass filter. This dc voltage is proportional to the intensity of the signal light incident on the PMT.

4.2.2. Homodyne-heterodyne detection

The case of two mixed fields with different, frequencies corresponds to heterodyne detection and as homodyne detection when the two frequencies are identical. Heterodyne detection allows a band-pass recovery of signal information centered at the frequency difference between the two mixed signals. Homodyne detection corresponds to the case where the local oscillator frequency equals the signal frequency.

In homodyne ANSOM, scattering from the sample is collected along with the scattering from the tip sample interaction without additional manipulation. It makes data difficult to interpret. Aubert analyzed homodyne ANSOM and found evidence of uncontrollable interfererence effects[67]. Gomez showed that the control of interferometric effect between the scattering from the tip and the back ground field can be controlled in heterodyne ANSOM[56].

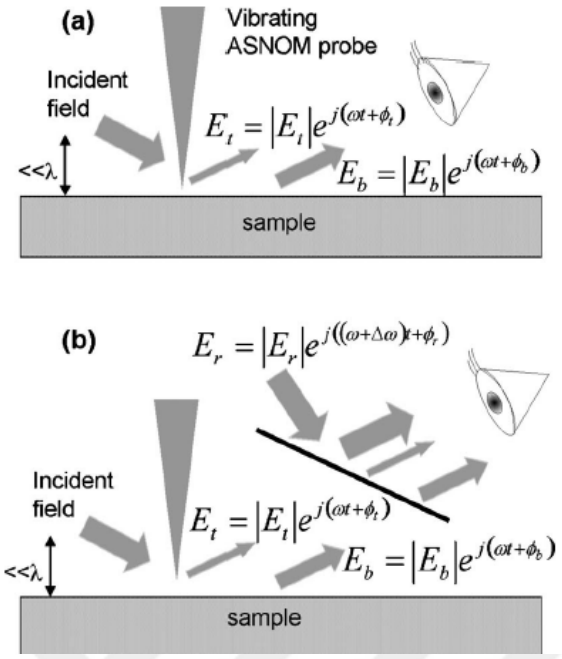

Figure 4.2 (a) Schematic configuration of a homodyne ASNOM. The detected light is the coherent superposition of the field scattered by the tip E_t and a background field E_b originating from the sample. (b) Schematic configuration of heterodyne ANSOM, where a frequency-shifted reference field Er is added to control the background signal[56].

In Figure 4.2 illumination and detection occur through far field geometry. E_b refers to scattering from the sample surface, and E_t refers to scattering from the tip extremity. In the equation

$$I = |E|^2 + 2|E_b||E_t|Cos(\Omega_t - \Omega_b) \quad (12)$$

I is the lock in detected signal at vibration frequency f or its harmonics nf in tapping mode AFM, and E_b and Ω_b are uncontrollable signals which vary during the scanning, it makes difficult to interpret data. On the other hand, in heterodyne type ANSOM, the interferometric signal can be controlled easily. Gomez proposed to replace

uncontrolled background field with a controllable reference field with a shifted frequency. By using a lock in frequency, variable background is eliminated[56].

The basic idea behind heterodyne detection is to replace the uncontrolled background field with a controllable reference field (E_r, ϕ_r) that is frequency shifted by $\Delta\omega$ relative to E_t. By doing that, a new lock-in frequency is used to eliminate the background signal.

The far field detected intensity is given by

$$I=I_1+I_2+I_3+I_4+I_5+I_6 \tag{13}$$

Where I_1, I_2, and I_3 are refer to the respective intensities of the different fields. Only $I_3 = |E_t|^2$ is time varying and can be extracted by lock-in detection. The signals E_b and E_r are filtered out. The fourth term I_4 refers to interference between the background and the scattered field from tip. The fifth term corresponds to interference between reference and background fields. The last term in the equation is the interference between E_t and the reference field, independent of the background field[68]. I_6 can be expressed as a Fourier series it can be expressed by:

$$I_6 \sim |E_t||E_r| Cos[(2\Omega \pm \Delta w)t + \varphi_r - \varphi_t] \tag{14}$$

where $\Omega=2\pi f$.

By performing lock-in detection at a frequency $(2\Omega - \Delta\omega)/2\pi$, the amplitude channel of the lock-in amplifier provides the amplitude of the tip field independently of the back ground field. Also, this amplitude can be enhanced by an adjustable factor E_r[68].

4.3. Surface Plasmon Polariton

A collective oscillation of electrons or a plasma wave near the surface of a metal is known as a surface plasma wave. The speed of a surface polariton is slower than the speed of light and it causes electromagnetic field to evanesce. Since the surface plasmon polariton is associated with an evanescent field, it can be excited by irradiation with an evanescent light wave satisfying the dispersion relationship at the boundary between the metal and the dielectric[69]. A sharp metallic tip plays an important role in the localized field enhancement, which is attributed to surface plasmon polaritons (SPPs) confined in the close vicinity of the tip apex.

In ANSOM, light polarized along the sharp axis of a metallic tip induces a high concentration of surface plasmons that results in strong enhancement of the electromagnetic field in the local vicinity of the tip. This localized enhancement in the light field has been widely applied in the near-field imaging of single molecules[70].

4.4. Internal and external geometry

The incident light is split into two beams by BS1. The transmitted beam, the reference field Er, is frequency shifted by two crossed acousto-optical cells and is coupled to a single-mode fiber. The beam reflected from BS1 is directed through a lens combination (L3 and L1) and is focused on the tip extremity by the objective O. The scattered light originating from the tip–sample (E_t+E_b) is collected by the same

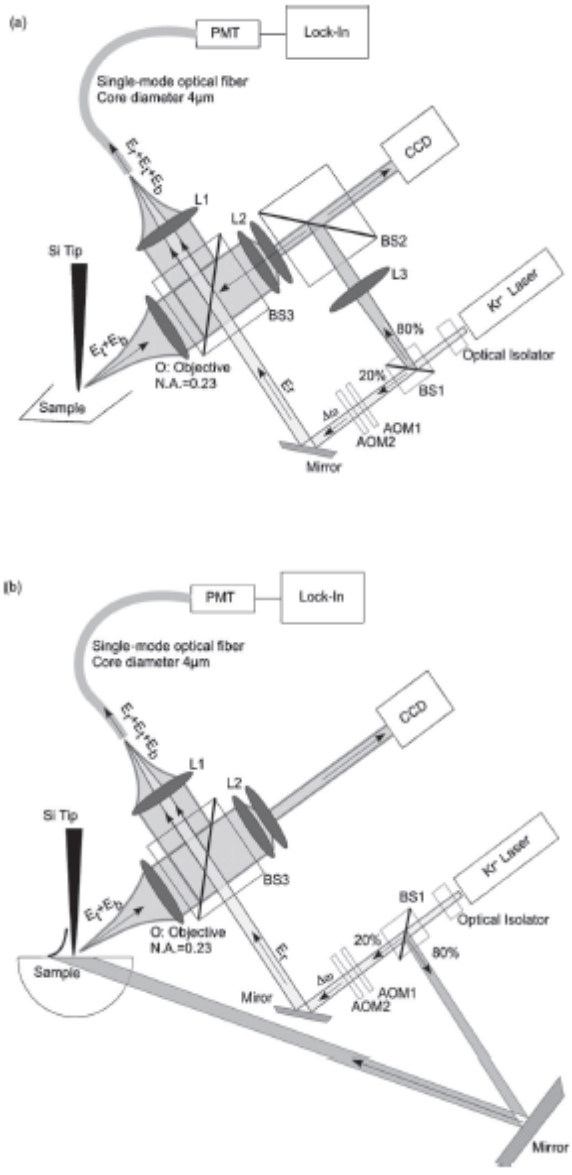

Figure 4.3 Details of the reflection-mode backscattered heterodyne setup.

objective O and is partially coupled to the optical fiber. The remaining fraction of the scattered light is imaged on a CCD camera for alignment purposes. The signals E_t, E_b, and E_r then interfere in the fiber, and the modulation is lock-in detected is shown in Figure 4.3. Details of the heterodyned apparatus for an evanescent illumination of the tip–sample is shown in Figure 4.3-b. The evanescent excitation is performed through total internal reflection inside an hemispherical lens. The heterodyne detection is essentially the same as in Figure 4.3-a.

External Geometry of ANSOM

Boccara presented a new apertureless near-field optical microscopic technique working in the transmission mode (1999). It works over the entire visible range of wavelengths[71]. He demonstrated that with this technique 5 nm lateral resolution can be achieved by analyzing optical signal with a simple model where the probe is assumed to be passive[70].

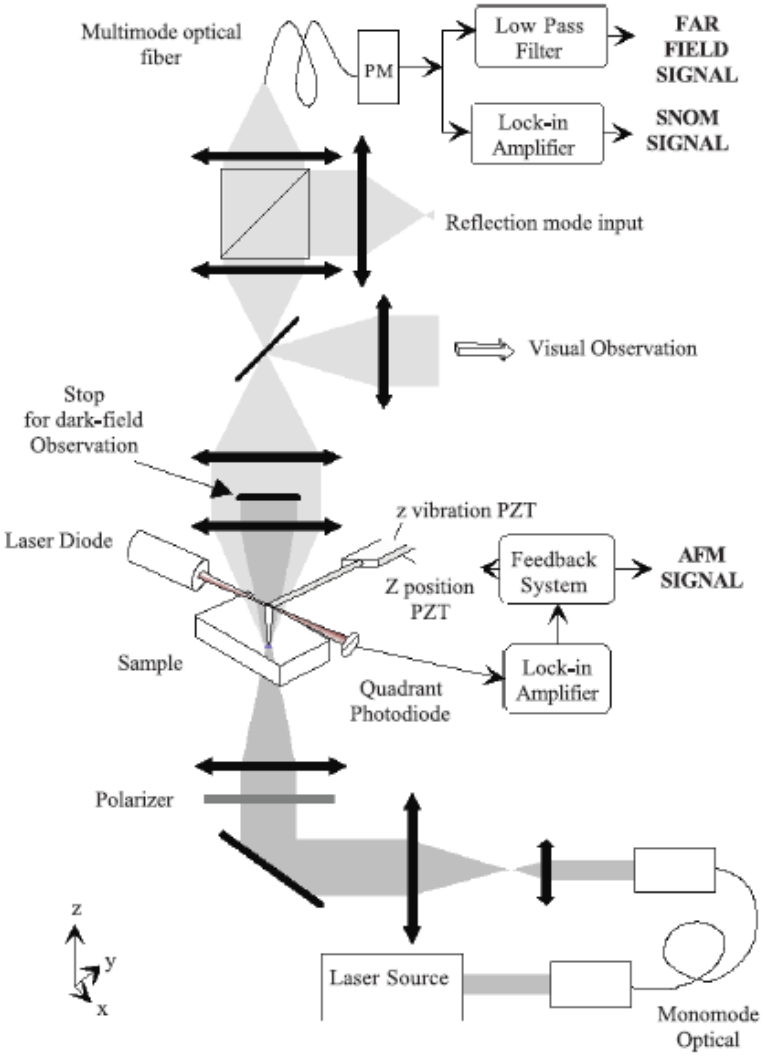

Figure 4.4 Experimental set-up of transmission-mode apertureless near-field microscope. PZT, piezo-electric transducer; PM, photomultiplier [71].

4.5. Antenna Effect on tip

Near-field optics and antenna theory have some similarities. The metal probes used in near-field microscopy are referred to as optical antennas since the tip functions similar to electromagnetic antennas. The relation of near-field optical microscopy with

antenna theory was considered by Wessel (Wessel, 1985)[72]. Keilmann 1995 and Novotny 1998 applied antenna model to near-field optics. In near-field optical microscopy the near-field probe can act as both a receiving antenna for localizing optical energy and a transmitting antenna for emitting the optical response. The antenna is a device which converts the energy of the propagating radiation into localized energy called feedback. In the feedback, electric circuitry either releases or receives the signal associated with the electromagnetic field. In ANSOM, an optical antenna basically replaces a conventional focusing lens, thereby concentrating external laser radiation in a region much smaller than the diffraction limit.

The illuminating tip should be focused exactly onto the tip, in a spot of about one wavelength λ diameter. However, this is still much larger than the dimensions of the tip apex as mentioned under field enhancement in Figure 4.1. In order to enhance the confined electric field at the tip apex over the incident field, the tip contributes as an antenna[73, 74]. In strong scattering the interaction between the probe and the excited field dominates. Thus, the probe acts as an optical antenna. The primary function of a near-field probe is the concentration of electromagnetic energy to a sample surface. The challenge of an antenna is to efficiently couple the power flow between the near-zone and the far-zone of the source[75].

Conclusion

Scanning tunneling microscopy has significantly contributed to our understanding of the fundamental structural and electronic properties of individual and bundled SWCNT. Studies of the SWCNTs in ambient condition have shown that the electronic properties of nanotubes depend on the metallic or semiconducting type of tubes. We have investigated the electronic properties of both metallic and semiconducting SWCNTs analyzing density of states. We showed that 10% of the nanotubes are semiconducting, and 90 % are metallic nanotubes. This is not the expected result for the ratio between metallic to semiconducting nanotubes which is 2/3 of total number of tubes in a bundle. Since we did not use ultra high vacuum STM, we could not prevent water exposure to the sample. For this reason the metallic behavior does not mean that the tubes are metallic. They can be semiconducting SWCNTs covered by a water layer. Due to the water layer the conductivity between the STM tip and the nanotubes increases, resembling with metallic behavior. Odom and Kim studied the DOS of SWCNTs in UHV-STM for both metallic and semiconducting tubes. However, in order to determine the metallic and semiconducting behavior of SWCNTs, it is not necessary to use UHV-STM. In ambient conditions we were able to determine the electronic properties of SWCNTs. Also, the low ohmic contact leads to metallic-like behavior for all carbon nanotubes. Our data is consistent with Dekker's results on the DOS of SWCNT in low-resistivity contact.

REFERENCES

1. Engel, T., Quantum chemistry and spectroscopy.
2. R.M. Feenstra, J. A. S. a. A. P. F., Tunneling spectroscopy of the Si(111) 2x1 surface. *Surface Science* **1986,** 181, p.295-306.
3. http://www.bphys.uni-linz.ac.at/bioph/download/Principles%20of%20Atomic%20Force%20Microscopy.
4. Binnig, G., C.F. Quate and C. Gerber,, Atomic Force Microscope. *Physical Review Letters* **1986,** 56, (9), p. 930.
5. http://www.spmtips.com/probes/triang/c11.
6. SUMIO, I., Discovery of Carbon Nanotubes. *Journal of the Institute of Electronics* **1999,** 82, (1), 12-16.
7. Scanning Probe Microscopy Studies of Carbon Nanotubes. In Heidelberg, Ed. Springer Berlin 2001; Vol. 80/2001.
8. Bharat Bhushan, H. F., *Applied Scanning Probe Methods II*. Springer Berlin Heidelberg: 2006; p 165-203.
9. T.W. Odom, J., L. Huang, P.Kim, C.M. Lieber, Structure and Electronic Properties of Single-Walled Carbon Nanotubes. . *Nature* **1998,** 391, 62.
10. Pavel Nikolaev, M. J. B., R. Kelley Bradley, Gas-phase catalytic growth of single-walled carbon nanotubes from carbon monoxide. *Chemical Physics Letters* **1999,** 313, 91-97.
11. Feenstra, R. M., Tunneling spectroscopy of the Si(11102x1 surface. *surface science* **1987,** 181, 295-306.
12. Teri Wang Odom, J.-L. H., Philip Kim, and Charles M. Lieber, Structure and Electronic Properties of Carbon Nanotubes. *J. Phys. Chem. B* **2000,** 104, 2794-2809.
13. M. E. Itkis, S. N., M. E. Meng, M. A. Hamon, H. Hu, and R. C. Haddon*, Spectroscopic Study of the Fermi Level Electronic Structure of Single-Walled Carbon Nanotubes. *NANOLETTERS* **2002,** 2, (2), 155-159.
14. S. NIYOGI, M. A. H., H. HU, B. ZHAO, P. BHOWMIK, R. SEN, M. E. ITKIS, AND R. C. HADDON, Chemistry of Single-Walled Carbon Nanotubes. *Acc. Chem. Res.* **2002,** 35, 1105-1113.
15. Kataura H., K. Y., Achiba Y. , Optical properties of Single Wall carbon nanotubes. *Synth. Met* **1999,** 103, 2555-2558.
16. Ouyang, M., Energy Gaps in "Metallic" Single-Walled Carbon Nanotubes. *Science* **2001,** 292, (702).
17. Zhen Yao, C. L. K., and Cees Dekker, High-Field Electrical Transport in Single-Wall Carbon Nanotubes. *Physical Review Letters* **2000,** 84, (13).
18. T.W. Odom, J., L. Huang, P.Kim, C.M. Lieber, Structure and Electronic Properties of Single-Walled Carbon Nanotubes. *Nature* **1998,** 391, 62.
19. Chen, J. H., M. A.; Hu, H.; Chen, Y.; Rao, A. M.; Eklund, P.C.; Haddon, R. C., Solution Properties of Single-Walled Carbon Nanotube. *Science* **1998,** 282, 95-98.
20. Itkis, M. E. N., S.; Meng, M.; Hamon, M.; Hu, H.; Haddon, R. C.F., Bohren, Spectroscopic Study of the Fermi Level Electronic Structure of Single Walled Carbon Nanotubes. *Nano Lett.* **2002** 2, (155-159).
21. Dresselhaus, M. S. D., Gene; Avouris, Phaedon *Carbon Nanotubes: Synthesis, Structure, Properties, and Applications*. 2001; Vol. 80
22. M. Ouyang, J. L. H., and C.M. Lieber, Fundamental Electronic Properties and Applications of Single-Walled Carbon Nanotubes. *Acc. Chem. Res.* **2002,** 35, 1018-1025.

23. Bin Zhao, H. H., Aiping Yu, Daniel Perea, and Robert C. Haddon*, Synthesis and Characterization of Water Soluble Single-Walled Carbon Nanotube Graft Copolymers. *J. Am. Chem. Soc.* **2005,** 127, 8197-8203.
24. M. E. itkis, S. N., M. E. Meng, M.A. Harmon, H. Hu, and R. C. Haddon, Spectroscopic Study of the Fermi Level Electronic Structure of Single-Walled Carbon Nanotubes. *Nano Lett.* **2002,** 2, (2), 155-159.
25. Leeuwenhoek, A. v., Published in the Philosophical Transactions of the Royal Society. *Letter to the Royal Society of London* **1683**.
26. Eric Betzig, J. K. T., Near-field optics- Microscopy, spectroscopy, and surface modification beyond the diffraction limit. *Science Direct* **1992,** 257.
27. D. Vobornik, G. M., J.S. Sanghera , P. Thielen , I.D. Aggarwal , B. Ivanovc, N.H. Tolk , V. Mannid, S. Grimaldi , A. Lisi , S. Rieti , D.W. Piston, Spectroscopic infrared scanning near-field optical microscopy (IR-SNOM). *Journal of Alloys and Compounds* **2005** 401, 80-85.
28. Bek, A., R. Vogelgesang, and K. Kern Apertureless scanning near field optical microscope with sub-10 nm resolution. *Review of Scientific Instruments* **2006,** 77, (4), 11.
29. F. Zenhausern, Y. M. a. H. K. W., scanning interferometric apertureless Microscopy:Optical imaging at 10 Angstrom Resolution. *Science* **1995,** 269, (5227), 1083-1085.
30. Synge, E. H., A suggested method for extending the microscopic resolution into the ultramicroscopic region. *Phil. Mag.* **1928,** 6, 356.
31. Synge, E. H., A suggested method for extending microscopic resolution into the ultramicroscopic region. *The London, Edinburgh, and Dublin Philosophical Magazine and Journal of Science* **1928,** 6, 7th series:356-362.
32. Kanemitsu, K. T. a. Y., Development of an Apertureless Near-Field Optical Microscope for Nanoscale Optical Imaging at Low Temperatures. *Japanese Journal of Applied Physics Part 1-Regular Papers Brief Communications & Review Papers* **2005,** 44, (1B), 575-577.
33. Bonnell, D., *Scanning Probe Microscopy and Spectroscopy:Theaory, Techniques, and Applications*. 2nd ed.; Wiley-VCH: New York, 2001.
34. http://www.physics.ncsu.edu/optics/nsom/NSOMintro.html.
35. F. Zenhausern 1, Y. M., and H. K. Wickramasinghe, Scanning Interferometric Apertureless Microscopy: Optical Imaging at 10 Angstrom *Resolution Science* **1995,** 269, (5227), p. 1083-1085.
36. http://www.reu.pdx.edu/PowerPoint%20Presenations/2007/Zechariah%20Dzegede.pdf.
37. Ewold Verhagen, J. A. D., L. (Kobus) Kuipers, Harry A. Atwater, and Albert Polman, Near-Field Visualization of Strongly Confined Surface Plasmon Polaritons in Metal-Insulator-Metal Waveguides. *Nano Lett.* **2008,** 8, (9).
38. F. Zenhausern, M. P. O. B., and H. K. Wickramasinghe, Apertureless near-field optical microscope. *Applied Physics Letters* **1994,** 65, (13), 1623-1625.
39. F. Zenhausern, Y. M., and H. K. Wickramasinghe, Scanning interferometric apertureless microscopy-optical imaging at 10 angstrom resolution. *Science* **1995,** 269, (5227), 1083-1085.
40. Y. Martin, S. R., and H. K. Wickramasinghe, Optical data storage read out at 256 Gbits/in2. . *Applied Physics Letters* **1997,** 71, (1), 1-3.

41. R. Bachelot, P. G., and A. C. Boccara, Near-field optical microscopy by local perturbation of a diffraction spot. *Microscopy Microanalysis Microstructures* **1994,** 5, (4-6), 389-397.
42. P. Gleyzes, A. C. B., and R. Bachelot, Near-field optical microscopy using a metallic vibrating tip. *Ultramicroscopy* **1995,** 57, (2-3), 318-322.
43. A. Lahrech, R. B., P. Gleyzes, and A. C. Boccara, Infrared-reflection-mode near-field microscopy using an apertureless probe with a resolution of λ /600. *Optics Letters* **1996,** 21, (17), 1315-1317.
44. Kawata, Y. I. a. S., Near-field scanning optical microscope with a metallic probe tip. *Optics Letters* **1994,** 19, (3), 159-161.
45. Inouye, S. K. a. Y., Scanning probe optical microscopy using a metallic probe tip. . *Ultra-microscopy* **1995,** 57, (2-3), 313-317.
46. Takashi Kodama, H. O., Development of new apertureless near-field scanning optical microscope tip using finite-differential time-domain calculation. *Chemical Physics Letters* **2006,** 432 553-557.
47. T. Kodama, T. U., S. Waatanabe, H. Othani, Development of ANSOM tips for the tip-enhanced raman spectroscopy. *Journal of microscopy* **2008,** 229, (2), pp-240-246.
48. Alpan Bek, R. V., and Klaus Kern Apertureless scanning near field optical microscope with sub-10□nm resolution. *Rev. Sci. Instrum.* **2006,** 77, (4).
49. Xiaobo Yin, N. F., and Xiang Zhanga, Near-field two-photon nanolithography using an apertureless optical probe. *APPLIED PHYSICS LETTERS* **2002,** 81, (194).
50. Y. Ogawa, F. M., Yohannes Abate, and Stephen R. Leone, Nanometer-scale dielectric constant of Ge quantum dots using apertureless near-field scanning optical microscopy. *APPLIED PHYSICS LETTERS* **2010,** 96, 063107.
51. Norihiko Hayazawa, K. F., Atsushi Taguchi, Satoshi Kawata, and Hiroshi Abe, Tip-enhanced two-photon excited fluorescence microscopy with a silicon tip. *APPLIED PHYSICS LETTERS* **2009,** 94, 193112.
52. Norihiko Hayazawa, K. F., 1 Atsushi Taguchi, Tip-enhanced two-photon excited fluorescence microscopy with a silicon tip. *APPLIED PHYSICS LETTERS* **2009,** 94, 193112.
53. Hori, M. O. a. H., *Near-Field Nano-Optics*. Kluwer Academic: Plenum, New York, 1999.
54. Zenhausern, F., Apertureless near-field optical microscope. *Applied physics letters* **1994,** 65, (13), 1623.
55. Wessel, J., Surface-enhanced optical microscopy. *J. Opt. Phys.* **1985,,** 2, (9), 1538-1541.
56. Lewis Gomez, R. B., Alexandre Bouhelier, Gary P. Wiederrecht, Shih-hui Chang, Stephen K. Gray, Feng Hua, Seokwoo Jeon, John A. Rogers, Miguel E. Castro, Sylvain Blaize, Ilan Stefanon, Gilles Lerondel, and Pascal Royer, Apertureless scanning near-field optical microscopy: a comparison between homodyne and heterodyne approaches. *JOSA B* **2006.,** 23, (5), p. 823-833.
57. Barbara P.F., A. D. M., characterizating of organic thin film materials with near-field scanning optical microscopy *Rev. Mater. Sci.* **1999,,** 29, 433.
58. Hillenbrand, R., Knoll B., Keilmann F., Pure optical contrast in scattering-type scanning near-field microscopy. *J. Microsc. Oxf.* **2001,** 202, 77-83.
59. Yinli Li, J. Z., Shifa Wu, Pengfei Li, and Shi Pan Comparison of AF/RSNOM with other RSNOM. *Chinese Optics Letters* **2005,** 3, (S1), pp. S316-S317.
60. Kawata, S., *Near-Field Optics and Surface Plasmon Polaritons*. Springer-Verlag Berlin Heidelberg: 2001.

61. Kawata, Y. I. a. S., Near-field scanning optical microscope with a metallic probe tip. *Optics Letters* **1994,** 19, (3), pp. 159-161.
62. A. BOUHELIER, J. R., M. R. BEVERSLUIS and L. NOVOTNY, Plasmon-coupled tip-enhanced near-field optical microscopy. *Journal of Microscopy* **2003,** 210, (3), pp. 220-224.
63. R. M. Roth, N.-C. P., M. M. Adams, R. M. Osgood, Jr., Plasmon-Resonant Field Enhancement Metallic Tip- Substrate Systems. *QELS*.
64. Kawata, Y. I. a. S., Image enhancement in near-field scanning optical microscopy with laser-trapped metallic particles. *Opt. Lett.* **1994,** 19, p. 159.
65. Winefordner, E. V. J. D., Basis and uses of Lock-in Detection in Analytical Spectrometry Instrumentation *Science&Technology* **1986,** 15, (4).
66. Satoru Fujime, S. C., Construction of a computer-Assisted Multichannel Lock-in detector. *Jpn. J. Appl. Phys.* **1980,** 19, (11), 2239-2244.
67. F. Formanek, Y. D. W., L. Aigouy, Analysis of the measured signals in apertureless near-field optical microscopy. *Ultramicroscopy* **2005,** 103,, (2), 133-139
68. Lewis Gomez, R. B., Alexandre Bouhelier, Gary P. Wiederrecht, Shih-hui Chang, and Stephen K. Gray, Apertureless scanning near-field optical microscopy: a comparison between homodyne and heterodyne approaches. *J. Opt. Soc. Am. B* **2006,** 23, (5).
69. Kawata, S., *Near-field optics and surface plasmon polaritons*. Springer: New York, 2001.
70. Tae-Hee Lee, J. I. G., and Robert M. Dickson, Strongly enhanced field-dependent single-molecule electroluminescence. *PNAS* **2002** 99, (16), 10272-10275
71. S Gr´esillon, H. C., J C Rivoal and A C Boccara, Transmission-mode apertureless near-field microscope: optical and magneto-optical studies. *J. Opt. A: Pure Appl. Opt.* **1999,** 1, 178-184.
72. Tim H Taminiau, F. B. S., Robert J Moerland, L (Kobus) Kuipers and Niek F van Hulst, Near-field driving of a optical monopole antenna. *J. Opt. A: Pure Appl. Opt.* **2007,** 9, S315-S321.
73. Markus Brehm, D. K., consolidating aperureless scaning near-field optical microscopy. *journal of the Korean physical society* **2005,** 47, pp S80-S85.
74. M. Brehm, A. S., F. Cajko, I. Tsukerman, and F. Keilmann,, Antenna-mediated back-scattering efficiency in infrared near-field microscopy. *Optics Express* **2008,** 16, (15), 11203-11215.
75. M. Brehm, A. S., F. Cajko, I. Tsukerman, and F. Keilmann, Antenna-mediated back-scattering efficiency in infrared near-field microscopy. *Optics Express* **2008,** 16, (15), pp. 11203-11215.
76. R. Bachelot, P. G. a. A. C. B., Near field optical microscope based on local perturbation of diffraction spot. . *Optics Letters* **1995,** 20, (18).